NAVAL POSTGRADUATE SCHOOL

MONTEREY, CALIFORNIA

THESIS

FLOWPATH DESIGN OF A THREE-TUBE VALVE-LESS PULSE DETONATION COMBUSTOR

by

Benjamin Zittere

September 2009

Thesis Advisor:	Jose Sinibaldi
Second Reader:	Chris Brophy

Approved for public release; distribution is unlimited

REPORT DOCUMENTATION PAGE			Form Approved OMB No. 0704-0188
Public reporting burden for this collection of information is estimated to average 1 hour per response, including the time for reviewing instruction, searching existing data sources, gathering and maintaining the data needed, and completing and reviewing the collection of information. Send comments regarding this burden estimate or any other aspect of this collection of information, including suggestions for reducing this burden, to Washington headquarters Services, Directorate for Information Operations and Reports, 1215 Jefferson Davis Highway, Suite 1204, Arlington, VA 22202-4302, and to the Office of Management and Budget, Paperwork Reduction Project (0704-0188) Washington DC 20503.			
1. AGENCY USE ONLY *(Leave blank)*	**2. REPORT DATE** September 2009	**3. REPORT TYPE AND DATES COVERED** Master's Thesis	
4. TITLE AND SUBTITLE Flowpath Design of a Three-Tube Valve-less Pulse Detonation Combustor		**5. FUNDING NUMBERS**	
6. AUTHOR(S) Benjamin D. Zittere			
7. PERFORMING ORGANIZATION NAME(S) AND ADDRESS(ES) Naval Postgraduate School Monterey, CA 93943-5000		**8. PERFORMING ORGANIZATION REPORT NUMBER**	
9. SPONSORING /MONITORING AGENCY NAME(S) AND ADDRESS(ES) N/A		**10. SPONSORING/MONITORING AGENCY REPORT NUMBER**	
11. SUPPLEMENTARY NOTES The views expressed in this thesis are those of the author and do not reflect the official policy or position of the Department of Defense or the U.S. Government.			
12a. DISTRIBUTION / AVAILABILITY STATEMENT Approved for public release; distribution is unlimited		**12b. DISTRIBUTION CODE**	

13. ABSTRACT (maximum 200 words)

This research investigates the effects of inlet dump angle on the size, shape, location and magnitude of recirculation zones for single side dump Pulse Detonation Combustor detonation tubes and describes the methods and results of hypothesized improvements to the internal flow path of those engines to ensure complete inter-cycle quenching. Additional analysis was conducted to visualize the dispersion of fuel along the feed tube and into the dump region as a means of providing initial validation of the design with respect to appropriate fuel concentration within the geometry.

14. SUBJECT TERMS PDE Pulse Detonation Engine Side Dump Combustor Recirculation Zone			**15. NUMBER OF PAGES** 77
			16. PRICE CODE
17. SECURITY CLASSIFICATION OF REPORT Unclassified	**18. SECURITY CLASSIFICATION OF THIS PAGE** Unclassified	**19. SECURITY CLASSIFICATION OF ABSTRACT** Unclassified	**20. LIMITATION OF ABSTRACT** UU

NSN 7540-01-280-5500 Standard Form 298 (Rev. 2-89)
Prescribed by ANSI Std. 239-18

THIS PAGE INTENTIONALLY LEFT BLANK

Approved for public release; distribution is unlimited

FLOWPATH DESIGN OF A THREE-TUBE VALVE-LESS PULSE DETONATION COMBUSTOR

Benjamin D. Zittere
Lieutenant Commander, United States Navy
B.S., University of Wisconsin, 1996

Submitted in partial fulfillment of the
requirements for the degree of

MASTER OF SCIENCE IN MECHANICAL ENGINEERING

from the

NAVAL POSTGRADUATE SCHOOL
September 2009

Author: Benjamin D. Zittere

Approved by: Jose Sinibaldi
Thesis Advisor

Chris Brophy
Co-Advisor

Knox Millsaps
Chairman, Department of Mechanical and Astronautical Engineering

THIS PAGE INTENTIONALLY LEFT BLANK

ABSTRACT

This research investigates the effects of inlet dump angle on the size, shape, location and magnitude of recirculation zones for single side dump inlet configuration in a Pulse Detonation Combustor. It also describes the methods and results of hypothesized improvements to the internal flow path of those engines to ensure complete inter-cycle quenching. Additional analysis was conducted to visualize the dispersion of fuel along the feed tube and into the dump region as a means of providing initial validation of the design with respect to appropriate fuel concentration within the geometry.

THIS PAGE INTENTIONALLY LEFT BLANK

TABLE OF CONTENTS

LIST OF FIGURES

THIS PAGE INTENTIONALLY LEFT BLANK

LIST OF TABLES

THIS PAGE INTENTIONALLY LEFT BLANK

EXECUTIVE SUMMARY

This research investigated the feasibility of using a single side-dump inlet arrangement in a Pulse Detonation Combustor. To probe the feasibility of this idea Computational Fluid Dynamics (CFD) models were run on the proposed geometry that has evolved from an operational symmetrically opposed four-inlet configuration. The conclusions are based on several incremental improvements in the models and predict that it is possible to use a single, unopposed inlet provided compensating modifications are made to the geometry to account for increased flow stresses on the ignition source. These conclusions are based solely on the analysis of viability of proper ignition and quench from the perspective of adequate fuel mixing and minimization of recirculation. Other factors such as thermal stresses on materials and joints, vibration of components and airstream particulate contamination were not examined and may play important roles in an operating device.

The two particular areas of investigation were recirculation zones in the vicinity of the igniter dispersion of fuel through the device, either of which could interfere with operation. The recirculation study used steady state models of cold flow within progressively advanced geometries to locate, characterize and reduce recirculation. The fuel dispersion study used transient models to analyze mass fraction of fuel as a function of position and time. Verification tests run after adjusting the injector geometry predicts that the fuel dispersion is acceptable.

THIS PAGE INTENTIONALLY LEFT BLANK

ACKNOWLEDGMENTS

This research was made possible by the team at the Rocket Propulsion Lab at the Naval Postgraduate School, led by Professor C. Brophy and including Mechanical Technician Mr. G. Hageman and Research Engineer Mr. D. Dausen.

The simulation and evaluation of data were guided and supervised by Professor Jose Sinibaldi.

Technical assistance and advice on the use of the STAR CCM+ software was provided by Mr. Jalil Farzin of CD-Adapco.

Support for this effort was provided by the Office of Naval Research under the direction of program manager, Dr. G. Roy

THIS PAGE INTENTIONALLY LEFT BLANK

I. BACKGROUND

A. INTRODUCTION

Multi-tube Pulse Detonation Engines (PDEs) represent a significant opportunity for reducing fabrication cost, increasing fuel efficiency, simplifying components and improving the range/payload options of future missile systems operating in supersonic conditions. The transition of the system to a newly attainable thermodynamic cycle will provide a step increase in thermodynamic efficiency between 10 and 20 percent. Such efficiency gains can be used to drive the same mass farther on a similar amount of fuel or a heavier mass the same distance. The cost will be reduced by simplifying the type of components required to operate the system and limiting their number. Specifically, for a multi-tube pulse detonation engine that can provide vectorable thrust, no moveable fins will be required.

As part of a brief comparison of Pulse Detonation technology to other forms of propulsion, a standard metric must be used to contrast one approach to another. Specific impulse (I_{sp}) is a measure of fuel efficiency representing the change in momentum per unit of fuel consumed and is defined as:

$$I_{sp} = F_{net}/m_f g$$

where

F_{net} = net thrust

m_f = mass flow rate of the fuel

g = gravitational constant

These specific impulse values vary by Mach number within each engine typology. When examples of various engine performance envelopes are plotted, they can be compared, as shown in Figure 1.

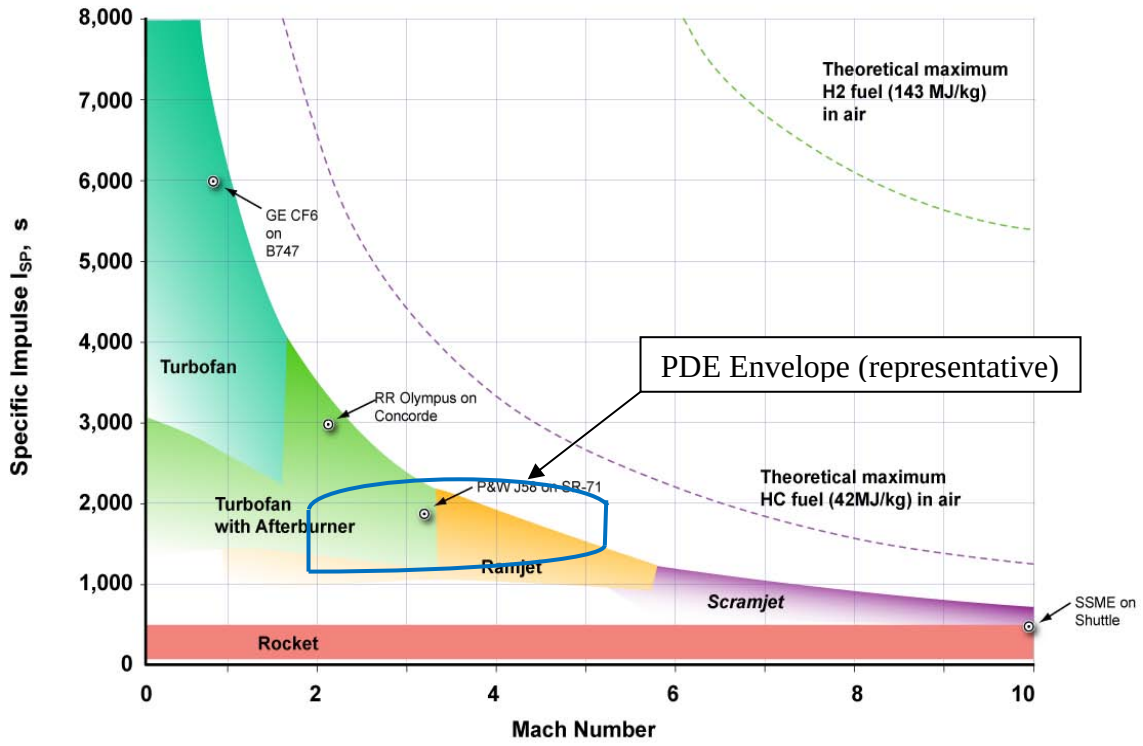

Figure 1. Reference Diagram for Engine Performance (Specific Impulse), from [1]

Pulse Detonation Engines can perform well at high efficiency across a large range of Mach numbers of practical interest for current systems. They compare favorably with current engine typologies in many aspects since they can operate at high efficiency from the transonic (Mach 0.8-1.2) region to high in the supersonic (Mach 1.0-5.0) region. Additionally, as they are still in the early stages of development, they have a large potential for gradual improvement that is not available with more mature technologies like gas turbines.

It is important to note that a Pulse Detonation Engine, like a Ramjet, relies on forward movement to compress the intake air and therefore cannot operate from rest. It will require some alternate propulsion device to accelerate the unit into the transonic region. This could be accomplished by using a booster rocket, for example.

B. ENGINE OPERATION

PDEs, of which the Pulse Detonation Combustor is the operational core, are superficially similar to Ramjets in that they use their forward motion to ingest air, which pressurizes as it slows in the internal ducting. They then mix in fuel and combust the mixture to produce high enthalpy combustion products and, subsequently, thrust. The primary difference between the Ramjet and the PDE is the nature of the combustion, which differs in two important ways. Firstly, the combustion in a Ramjet is a deflagration (subsonic combustion) whereas in the PDE the combustion is a detonation (supersonic combustion). Additionally, the ramjet operates at steady state, injecting fuel at a nearly constant rate and maintaining a stable flame. The PDE by contrast operates in an intermittent manner by injecting short charges of fuel into a constant airstream. This fuel mixes with the air to form a combustible mixture that is then detonated. Detonation occurs when a high-energy deflagration accelerates to supersonic velocities, thus producing a leading shock wave. This process is known as Deflagration-to-Detonation Transition (DDT). A more thorough explanation of this process for the specific case of the operation model is presented in the Detonation Obstacles section E. on page 10. After the detonation event is complete, the continuous flow of air purges the chamber, quenching the remaining combustion products and preparing the engine for a subsequent cycle. Engines being operated at the time this thesis was written complete approximately 50 to 100 cycles per second. The combustors modeled in this thesis are also expected to perform at this rate.

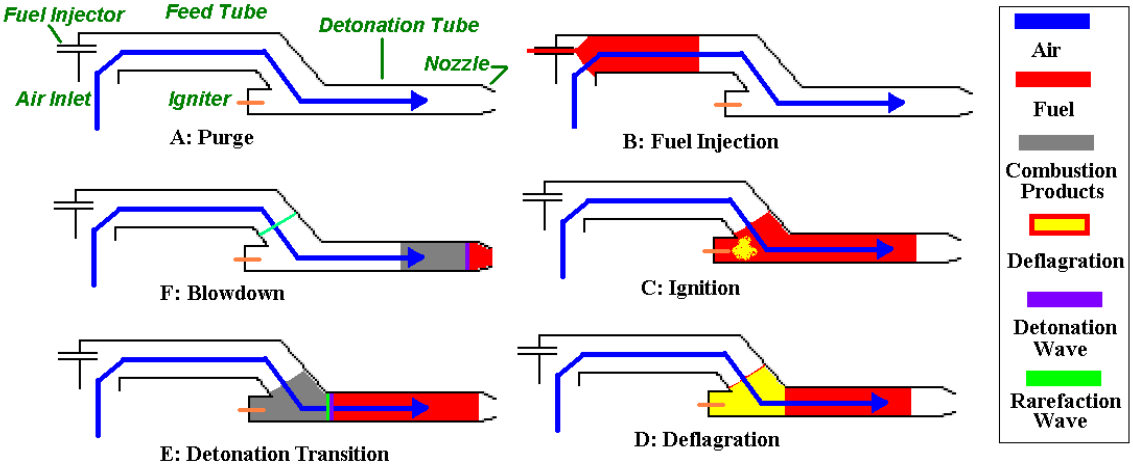

Figure 2. PDC Cycle Diagram

The PDC cycle consists of six phases, as depicted in Figure 2.

1. A continuous flow of pressurized air flows through the injector section, feed tube and detonation tube.
2. Fuel is supplied to the combustor through the injection port and diffuses into the airstream.
3. The fuel air mixture is ignited.
4. Combustion proceeds by deflagration
5. Combustion transition to Detonation
6. Waves dissipate and fresh air purges the system, returning it to the beginning of the cycle.

PDCs can be integrated into a system to produce either thrust or mechanical power. In a thrust producing engine, the operation is as described above. To extract shaft power, the engine is configured much like a gas turbine, with a leading compressor operating off of spool power, to provide high pressure inlet air. The core of the engine operates as above, but instead of using a single nozzle to convert pressure to kinetic energy (thrust) the pressure is used to turn a turbine. The turbine shaft output is mechanical energy, some of which is consumed to power the front-end compressor.

In both cases, using a detonation-based instead of a deflagration-based combustion cycle theoretically increases the fuel efficiency and performance of the machine as described by the thermodynamic characteristics stated above and described below.

C. THERMODYNAMICS OF DETONATION

Combustion of the fuel-air mixture via a detonation vice a deflagration allows the thermodynamic process to be modeled as a near constant volume instead of constant pressure combustion. The detonation event consists of a high-speed supersonic combustion wave that rapidly traverses the combustor resulting in a nearly constant volume energy release process. This compares favorably to the constant pressure process utilized in traditional gas turbine engines since the detonation event produces a lower entropy rise and more available work than a Brayton cycle operating at similar conditions. The working fluid in a pulse detonation combustor has often been modeled to execute the Humphrey cycle. This cycle includes four processes, which can be observed by referencing the diagram in Figure 3:

- Isentropic compression (1-2)
- Constant volume combustion (2-3)
- Isentropic expansion (3-4)
- Isobaric heat rejection (4-1)

In a traditional gas turbine engine, the combustion is more appropriately modeled as a constant pressure process (Brayton cycle), with the result that the combustion process ends at state 3a vice state 3.

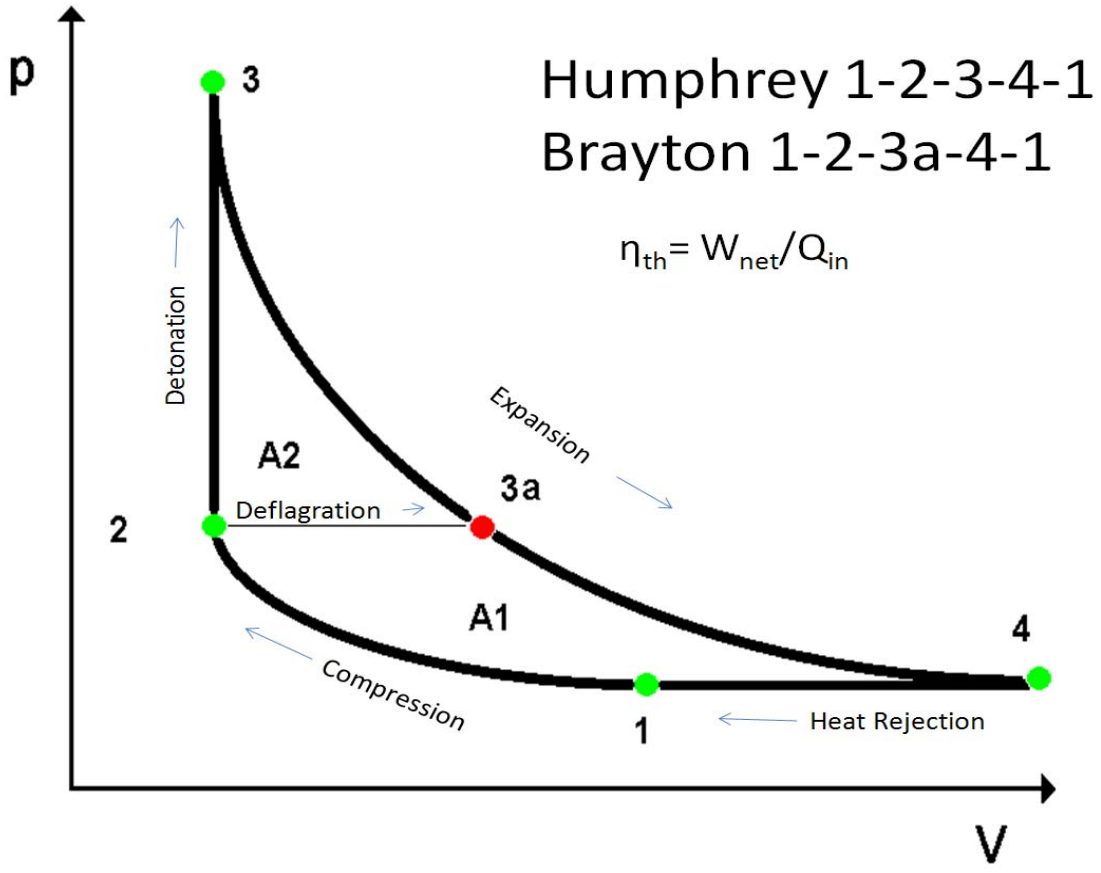

Figure 3. Pressure – Volume Diagram of Humphrey Cycle

The areas A1 and A2 in the above diagram represent the amount of work extracted from their respective processes per cycle. In the Brayton cycle, represented by A1, there is a significantly lower yield when compared to the Humphrey cycle, which envelops area A1+A2. It is important to remember that, for the comparison to be meaningful, the cycles must be consuming the same amount of fuel.

This change in operating points from 3a to 3 extracts additional energy from each unit of fuel consumed. The additional energy yield causes thermodynamic efficiency to increase.

Thermodynamic efficiency is defined by the following relation:

$$\eta_{th} = \frac{W_{net}}{Q_{in}}$$

where

W_{net} = System net work output

Q_{in} = Energy input to the system

The higher thermodynamic efficiency translates into some combination of increased payload, longer range and a decreased weight for a propulsion system.

The existing PDC at the Naval Postgraduate School consists of a single tube with multiple opposed inlets in the vicinity of an igniter contained in a domed head. The geometry of this setup encompasses drawbacks that can potentially prevent achieving reliable detonations from cycle to cycle if the design were modified to utilize a single inlet. Recirculating vortices in the flow can potentially prevent effective purging in the regions adjacent to the igniter. These recirculating zones could capture previous cycle hot products and cause premature ignition of fresh fuel-air reactants in subsequent cycles, which would drive the system away from detonation. This would negate the benefits of using pulsed detonation in the first place, and needs to be avoided.

A more detailed explanation of this topic is provided by Heiser and Pratt [2].

D. PULSE DETONATION ENGINE TERMINOLOGY AND GEOMETRY

Figure 4 shows the current PDC configuration at NPS. The flow moves from right to left in this schematic.

1. Current Geometry

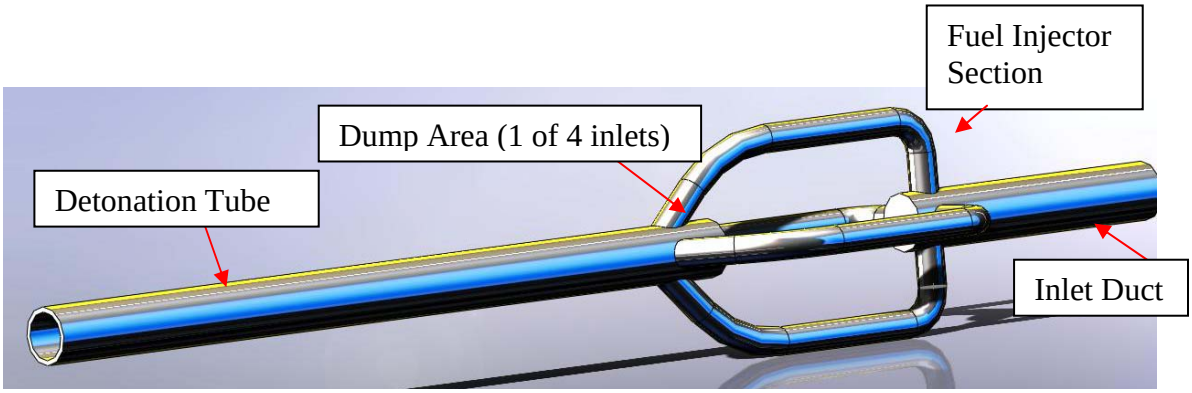

Figure 4. PDE Terminology Diagram (Four-Inlet Geometry)

2. Proposed New Geometry

a. Whole Rig Geometry

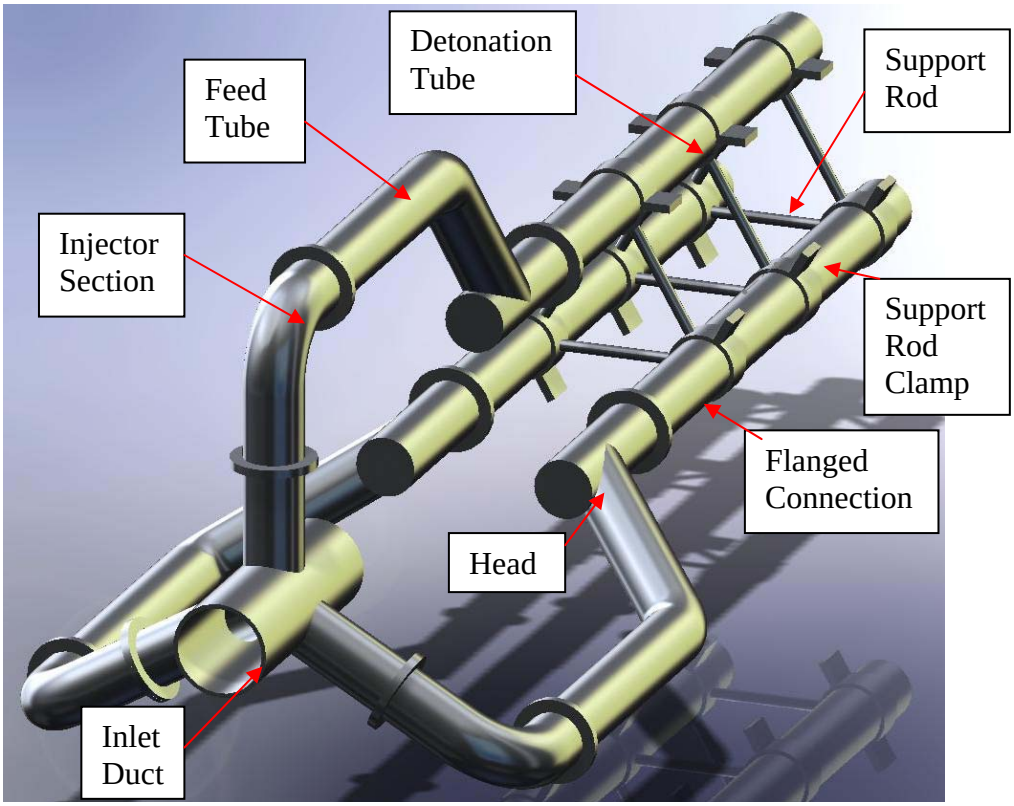

Figure 5. PDE Terminology Diagram (3 tube rig – single inlet per tube)

The multi-tube configuration assembly shown in Figure 5 consists of three combustors, associated individual injectors and inlet arms, all connected to a larger central inlet duct. The rig also includes the structures required to mechanically couple and support the individual components such as flanged attachments and clamped support rods

b. Single Branch Geometry

Each single inlet arm contains all components downstream of the flanged connection on the inlet duct; injector section, injector elbow, feed tube, igniter and igniter shroud, detonation tube and nozzle. Interaction effects between individual detonation tubes are limited by the choking of flow upstream. Modeling of single branches makes

use of the symmetric nature of the rig to allow a great reduction in computational complexity without sacrificing model accuracy. Follow on work may require total rig modeling to validate the predictions of isolation from interaction effects, but that is beyond the scope of this thesis. The nomenclature for each single branch is identical and includes the Injector section, feed tube/inlet arm, detonation tube and nozzle as well as all interior components such as the igniter, shroud and detonation initiation ramps.

c. Detail of Inlet Arm / Detonation Tube with Igniter Area

The inlet manifold arm transfers the air from the inlet plenum, past the injector and into the igniter region of the detonation tube at the required dump angle relative to the detonation tube axis as depicted in the detailed view in Figure 6. The igniter and shroud assembly provide a region of lower velocities with rapid electrical energy deposition to initiate the reaction. The head region of the detonation tube houses the igniter and shroud, allowing them to operate under more favorable conditions and avoid the high stresses inherent in cross flow that could be detrimental to brittle igniter materials. In later designs the head is reduced, and then removed to facilitate the removal of recirculation in the vicinity of the igniter and shroud.

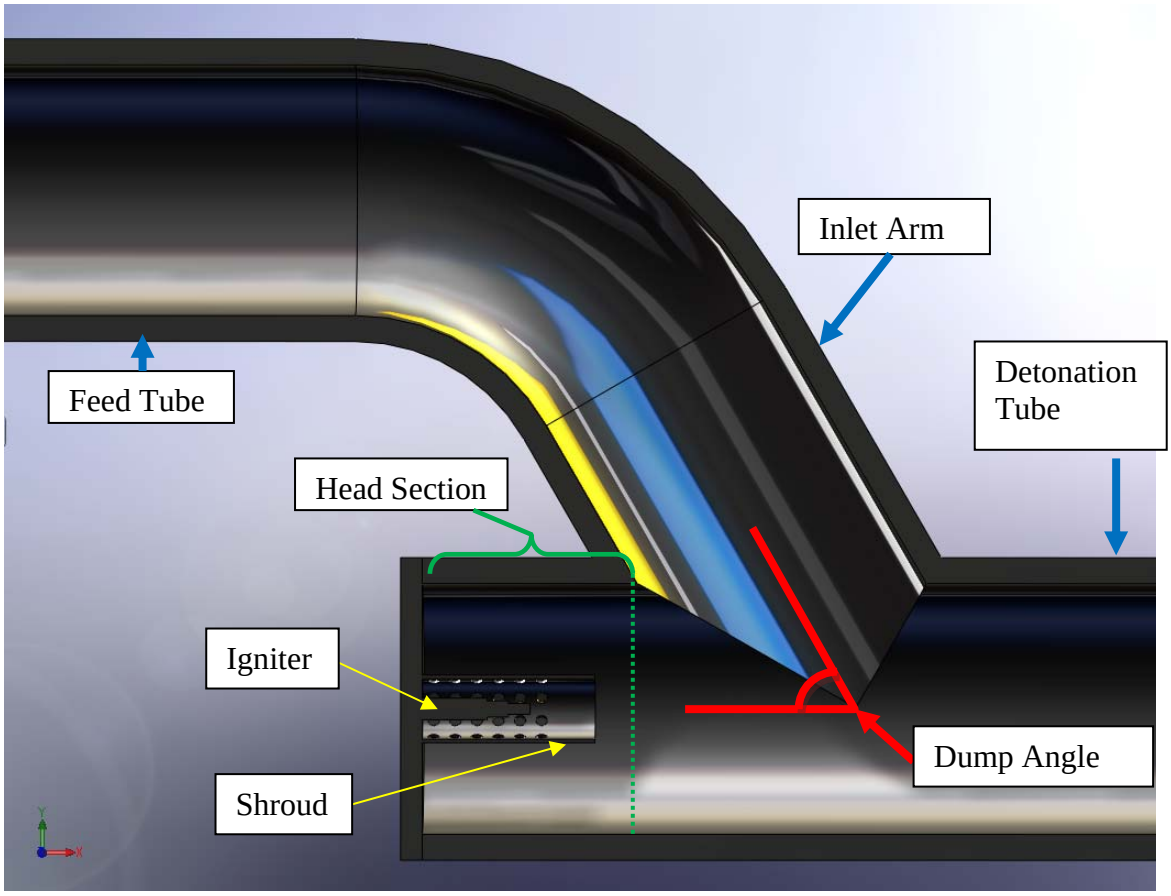

Figure 6. PDE Terminology Diagram (detail section view)

d. Head Geometry

The head section is that portion of the detonation tube upstream of the inlet. It houses the igniter and shroud. Variations of this configuration are displayed in Figures 7 and 8.

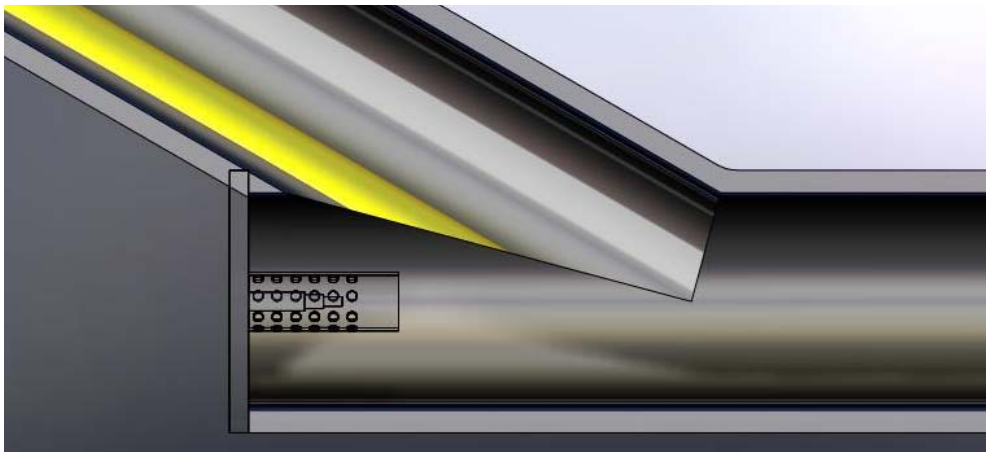

Figure 7. Semi-Headless Design (detail section view)

The semi-headless design shortens the head length until the wall nearest the inlet tube reaches negligible length.

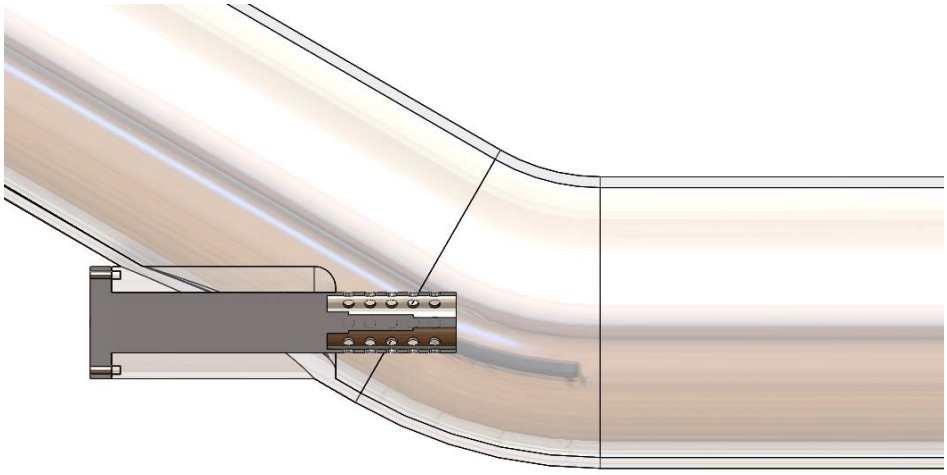

Figure 8. Headless Design (detail section view)

In the headless design above, the dump angle is still the angle made by the axes of the inlet tube and the detonation tube; for consistency of nomenclature with previous models, however, the base of the angle is measured from the direction of the absent head-end region. The elimination of the head-end region places the igniter and shroud in a more energetic flow, which requires they be able to withstand higher stresses.

E. DETONATION OBSTACLES AND DDT

Part of the overall project involves ensuring the reliable transition from deflagration-to-detonation while maintaining a low-pressure loss through the detonation tube. The DDT process is summarized by Kenneth Kuo in Principles of Combustion [3] as a seven-step series of events as follows:

1. Generation of compression waves ahead of an accelerating laminar flame
2. Formation of a shock front due to coalescence of compression waves
3. Movement of gases induced by shock causing the flame to break into a turbulent brush
4. Onset of "an explosion in an explosion" at a point within the turbulent reaction zone, producing two strong diverging shocks
5. Development of a spherical shock wave near the boundary layer
6. Interaction of transverse waves with the shock front and reaction zone
7. Establishment of a final "steady wave" culminating in self sustained detonation

The details of the transition are not particularly germane to the overall flow path other than to recognize that some sort of obstacle will be needed to induce transition, and the design will need to account for any effects produced by those obstacles.

1. Detonation Inducing Obstacles (Swept Ramps)

Parallel research undertaken by LT Travis Dvorak is investigating specific geometries intended to accomplish this transition. As of the writing of this thesis, however, the best obstacle geometry available is a pair of two linear series of swept ramps (shown in Figures 9 and 10).

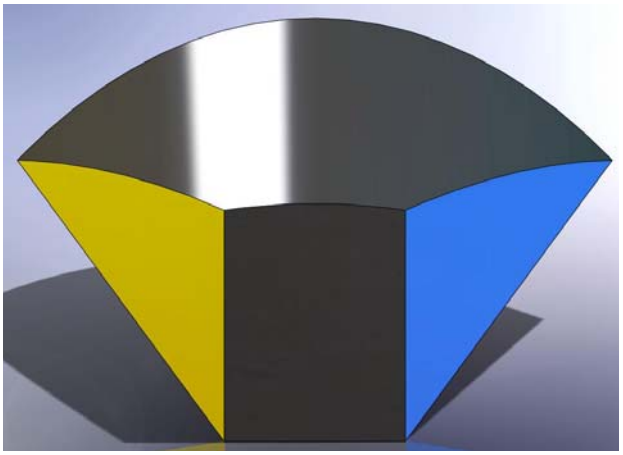

Figure 9. Detonation Obstacle, Ramp (downstream view)

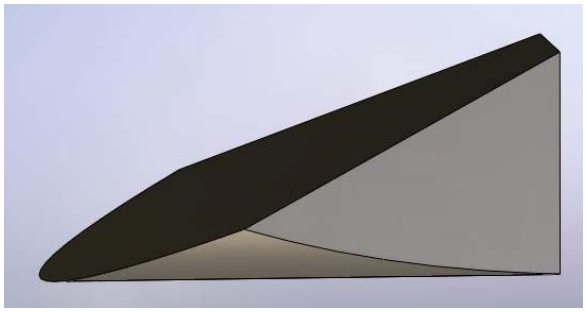

Figure 10. Detonation Ramp (side view)

2. Ramp Arrangement

The ramp above is fitted into the detonation tube (shown in Figure 11) with the curved side matching the interior of the tube wall. Flow passes from left to right in the side view causing large counter-rotating streamwise vortices that cause rapid flame acceleration, explosion events, and ultimately result in a detonation wave.

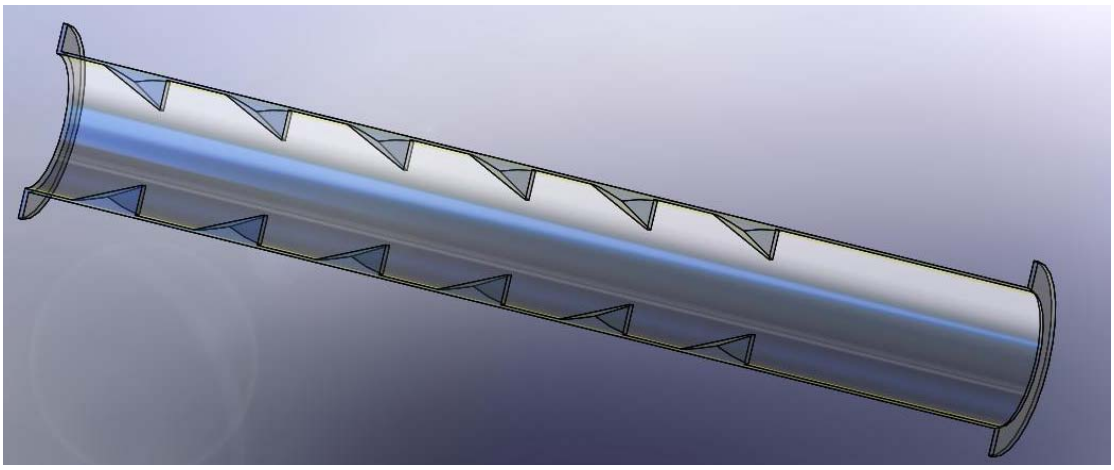

Figure 11. Detonation Ramp Layout (section view)

The series of ramps is arranged in two diametrically opposed lines in a saw-tooth pattern.

F. THRUST VECTORING

The use of multiple parallel detonation tubes as in the three-tube rig has many advantages over a single larger engine. Prominent among these advantages is the ability to combine the intermittent thrust properties of the individual engines and the geometric arrangement of the tubes off of the central longitudinal axis of the rig to turn the entire assembly without fins or auxiliary thrust producing mechanisms. This is accomplished by temporarily reducing the thrust produced by one of the three tubes while allowing the other two to maintain normal thrust. This thrust deficit, combined with the radial distance from the center axis of the rig to the center axis of the reduced thrust tube, will induce a torque on the entire assembly around the center of mass.

By allowing navigation / piloting system to interact with the fuel delivery system and impose some pattern of fuel reduction on specific combustors, the system could be steered via thrust vectoring.

G. PREVIOUS RESULTS (LITERATURE REVIEW)

The relative novelty of functional pulse detonation combustors limits the number of references available for direct information about the internal configuration, but similar characteristics of ramjet engines, along with their well researched and extensively documented development, provides several sources of useful information, specifically some relating to single side dump combustor design.

As the focus of this thesis on side-dump combustor inlet angle may suggest, the work of Yen and Ko [4] was useful in predicting the behavior of flow structures when varying the dump angle. Unfortunately, they were focused on dual inlets, which add a nominal plane of symmetry to the structure. Similarly, Nosseir and Behar [5] conducted a study in which the interaction of impinging flows from opposed dump inlets dominate the flow structure. Deppe's [6] work focused on Ramjet applications, which seek to promote recirculation in the vicinity of the igniter to ensure steady state combustion without the need for a continuous ignition source. While all of these sources held useful insights, none would sufficiently predict behavior of an unopposed inlet.

H. THEORY (FLUID MECHANICS)

Overviews of rotational and recirculation zones associated with geometric discontinuities in high-speed flows are available from many sources.

1. Phenomena

The two most germane phenomena are the reverse step flow scheme and the bent pipe flow scheme. Of additional, but not primary interest, is the cylinder in cross-flow. This third phenomenon is more pronounced in the headless design.

2. Recognized Structures

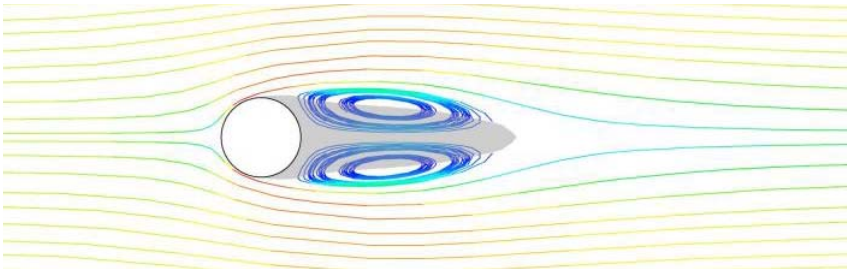

Figure 12. Flow structures downstream of a cylinder in cross-flow

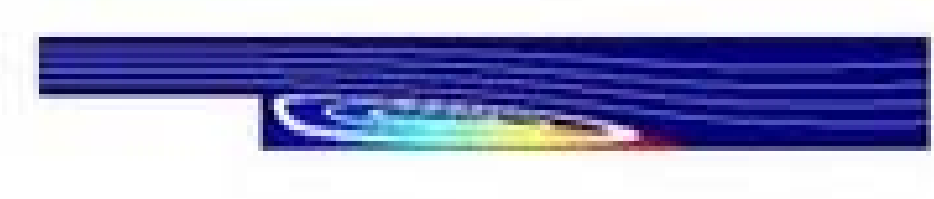

Figure 13. Recirculation zone over a backstep

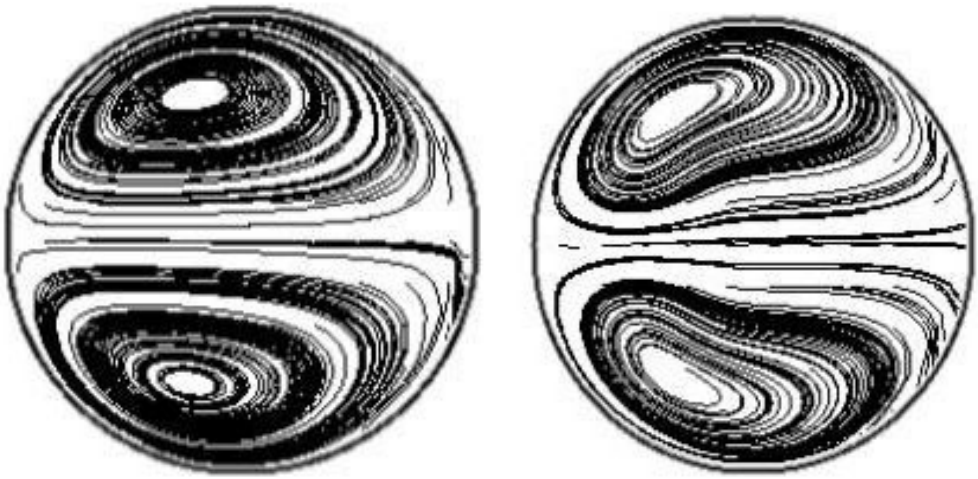

Figure 14. Flow structures after a pipe bend (at 45 and 90 degrees)

Note that in these three fluid-boundary interactions rotational flow structures are generated. In the cases of the crossflow cylinder and the backstep, the axis of rotation is in a transverse direction (perpendicular to the predominant flow direction) whereas in the

bent pipe, these structures rotate longitudinally along the path of the primary flow. To visualize this, recognize that in the first two scenarios the fluid is flowing from left to right generating recirculating eddies whose curvature appears circular or elliptical in cross section. In the bent pipe, the primary flow is toward the reader (out of the page) and the circular structures represent slices of a helical vortex. It is believed that some aspect of these three basic structures is present in varying degrees in the models developed here and they will be utilized in the explanation of model results.

I. OBJECTIVES

The goal of this research is to provide a functional sub-scale pulse detonation combustor system that can demonstrate variable thrust vector control. Among the many technical challenges involved in this goal are: detonation modeling, fuel injection/evaporation modeling, igniter flow modeling, detonation tube geometry design and exit nozzle design. Pursuant to this goal several students are conducting research on various aspects of the larger problem including nozzle design, detonation tube obstacle design to enhance deflagration-to-detonation transition and internal flow path design. Experiments are conducted on an instrumented simple combustor comprised of a single main tube with four opposed inlet arms. The main tube includes an interchangeable section that contains initiation obstacles. The results of these combustor experiments are used to validate computational predictions.

The objective of this work was to investigate the feasibility of using a combustor with a single side-dump inlet. It was desirable to avoid excessive recirculation zones in the vicinity of the igniter, thus ensuring effective purge at the conclusion of each cycle. In pursuit of this objective, the effects of various dump angles (angle between the inlet arm and the detonation tube) on recirculation in the igniter region were explored. Additionally, the convection of fuel downstream of the injector was examined to predict viability of the single side-dump design with respect to cycle ignition.

THIS PAGE INTENTIONALLY LEFT BLANK

II. COMPUTATIONAL MODELING

A. CFD FUNDAMENTALS

1. Overview

Computational Fluid Dynamics permits a numerical solution to problems with no closed-form solution. This is accomplished by defining the physical region over which the solution is to be constructed, breaking the region into a number of small, discrete volumes, defining the governing equations that determine the relationships between adjacent cells, then imposing initial and boundary conditions on the solution. A simultaneous solution of the resulting matrix of equations yields a complete solution of the bounded physical space to the resolution of the initial grid.

2. Time and Distance Scale Relation

One of the major concerns for transient fluid analysis with this method is the Courant number. This dimensionless parameter correlates the size of the physical and time grid divisions by comparing them to the speed of sound in the operating fluid. From a mathematical standpoint, Courant numbers (commonly represented by the symbol λ) of less than one are stable because the time steps are sufficiently fine to allow variations in properties to propagate through the fluid and be appropriately accounted for. In this analysis the relevant numbers are:

$$\Delta x = 2.5e\text{-}3m$$

$$\Delta t = 1e\text{-}5\ s$$

$$c = 344\ m/s$$

$$\lambda = c\frac{\Delta t}{\Delta x} = \frac{\left(344\frac{m}{s}\right)(0.00001\ s)}{0.025\ m} = 1.376$$

This Courant Number allows a reasonable calculation rate and convergence.

3. Governing Equations

The equations used are the Euler and Navier-Stokes equations represented as Newton's second law (conservation of momentum), the continuity equation (conservation of mass), and the first law of thermodynamics (conservation of energy). Within each cell, properties of the fluid can be described by a low order Taylor series approximation about their central value. The fluid properties (temperature, pressure, density, etc.) are functions of space and/or time and the values at the boundaries can be solved for within a reasonable degree of precision with the first few terms of the Taylor series expansion. Since the border is shared by two cells, its value from one side must equal its value from the other. These properties allow the equations to be connected with a finite differencing scheme. Using the substantive derivatives, each property can be solved for as:

$$\frac{Dq}{Dt} = \frac{\partial q}{\partial t} + \frac{\partial q}{\partial x}\frac{dx}{dt} + \frac{\partial q}{\partial y}\frac{dy}{dt} + \frac{\partial d}{\partial z}\frac{dz}{dt}$$

where

q = any property

In problems where viscosity plays no significant role, that is, viscous forces are orders of magnitude lower than momentum or body forces, the Euler equations give good results while imposing lighter computational demands on the solver and system.

The equations used in the Euler approximation are:

Mass: $$\frac{\partial}{\partial t}\rho + \frac{\partial}{\partial x}\rho u + \frac{\partial}{\partial y}\rho v + \frac{\partial}{\partial z}\rho w = 0$$

X-Momentum: $$\frac{\partial}{\partial t}\rho u + \frac{\partial}{\partial x}\rho u^2 + \frac{\partial}{\partial y}\rho uv + \frac{\partial}{\partial z}\rho uw + \frac{\partial P}{\partial x} = 0$$

Y-Momentum: $$\frac{\partial}{\partial t}\rho v + \frac{\partial}{\partial x}\rho uv + \frac{\partial}{\partial y}\rho v^2 + \frac{\partial}{\partial z}\rho vw + \frac{\partial P}{\partial y} = 0$$

Z-Momentum: $\frac{\partial}{\partial t}\rho w + \frac{\partial}{\partial x}\rho uw + \frac{\partial}{\partial y}\rho vw + \frac{\partial}{\partial z}\rho w^2 + \frac{\partial P}{\partial z} = 0$

Energy: $\frac{\partial e}{\partial t} + \frac{\partial}{\partial x}(e + p)u + \frac{\partial}{\partial y}(e + p)v + \frac{\partial}{\partial z}(e + p)w = 0$

where

$e = \rho\left[C_v T + \frac{(u^2+v^2+w^2)}{2}\right]$ for an ideal gas.

If the problem seeks to include viscous forces, the full Navier Stokes equations must be solved. The mass and momentum equations are identical, but the energy equation includes many additional terms to account for the viscous dissipation of energy. This is essential to modeling turbulent flows.

Mass: $\frac{\partial}{\partial t}\rho + \frac{\partial}{\partial x}\rho u + \frac{\partial}{\partial y}\rho v + \frac{\partial}{\partial z}\rho w = 0$

X-Momentum: $\frac{\partial}{\partial t}\rho u + \frac{\partial}{\partial x}\rho u^2 + \frac{\partial}{\partial y}\rho uv + \frac{\partial}{\partial z}\rho uw + \frac{\partial P}{\partial x} = 0$

Y-Momentum: $\frac{\partial}{\partial t}\rho v + \frac{\partial}{\partial x}\rho uv + \frac{\partial}{\partial y}\rho v^2 + \frac{\partial}{\partial z}\rho vw + \frac{\partial P}{\partial y} = 0$

Z-Momentum: $\frac{\partial}{\partial t}\rho w + \frac{\partial}{\partial x}\rho uw + \frac{\partial}{\partial y}\rho vw + \frac{\partial}{\partial z}\rho w^2 + \frac{\partial P}{\partial z} = 0$

Energy:

$$\frac{\partial P}{\partial t}\frac{1}{\gamma-1} + \frac{\partial u}{\partial t}\frac{\rho u}{2} + \frac{\partial v}{\partial t}\frac{\rho v}{2} + \frac{\partial w}{\partial t}\frac{\rho w}{2} + \frac{\partial P}{\partial x}\frac{\gamma u}{\gamma-1} + \frac{\partial P}{\partial y}\frac{\gamma v}{\gamma-1} + \frac{\partial P}{\partial z}\frac{\gamma w}{\gamma-1} + \frac{\partial u}{\partial x}\left(\frac{\gamma P}{\gamma-1} + \frac{3\rho u^2+\rho v^2+\rho w^2}{2}\right) + \frac{\partial v}{\partial y}\left(\frac{\gamma P}{\gamma-1} + \frac{\rho u^2+3\rho v^2+\rho w^2}{2}\right) +$$

$$\frac{\partial w}{\partial z}\left(\frac{\gamma P}{\gamma-1} + \frac{\rho u^2+\rho v^2+3\rho w^2}{2}\right) + \frac{\partial \rho}{\partial t}\frac{(u^2+v^2+w^2)}{2} + \frac{\partial \rho}{\partial x}\frac{u^3+uv^2+uw^2}{2} + \frac{\partial \rho}{\partial y}\frac{u^2v+v^3+vw^2}{2} + \frac{\partial \rho}{\partial z}\frac{u^2w+v^2w+w^3}{2} + \frac{\partial v}{\partial x}\rho uv +$$

$$\frac{\partial w}{\partial x}\rho uw + \frac{\partial u}{\partial y}\rho uv + \frac{\partial w}{\partial y}\rho vw + \frac{\partial u}{\partial z}\rho uw + \frac{\partial v}{\partial z}\rho vw = 0$$

It should be noted that the simultaneous solution of matrices of non-linear partial differential equations with computers has only been made possible in the last 30 years and new schemes for representing the properties of fluids are still being developed as are new algorithms for solving those equations.

4. Models and Assumptions

To numerically solve the full Navier-Stokes equations is quite challenging computationally and is currently only employed on very small regions. This technique, known as direct numerical simulation (DNS) is realizable only for low Reynolds number flows across small regions of space and over short time spans. This is due to the requirement to resolve the entire range of turbulence scales without simplifying models. At the smallest (Kolmogorov) scales turbulent dissipation is regulated by the relationship between energy dissipation and kinematic viscosity as follows.

Table 1. Kolmogorov microscale parameters

Kolmogorov Length Scale	$\eta = \left(\frac{\upsilon^3}{\varepsilon}\right)^{\frac{1}{4}}$
Kolmogorov Time Scale	$\tau_\eta = \left(\frac{\upsilon}{\varepsilon}\right)^{\frac{1}{2}}$
Kolmogorov Velocity Scale	$u_\eta = (\upsilon\varepsilon)^{\frac{1}{4}}$

where

υ = kinematic viscosity

ε = energy dissipation

At larger scales the turbulence is characterized by the size of the largest eddies (designated L). This parameter is greatly affected by the physical boundaries of the system and must also be captured in the computational domain with sufficient resolution

to resolve the changing properties. Since the Courant criteria must still be satisfied, the computational burden imposed by direct numerical simulation grows as a function of Re^3 and is unsolvable for a project of this scale with even the most powerful computers currently available.

As an alternative, many turbulence models have been developed over the history of CFD to circumvent this problem. The most basic and most popular are a series of similar models known as the κ-ε turbulence models. These models introduce two additional equations to represent the transport of turbulence through the flow. The two variables are κ, the turbulent kinetic energy and ε, the turbulent dissipation. The interplay between the magnitude of turbulence energy and the dissipation of that same energy allows for reasonable estimations of the dispersion or turbulent energy throughout the flow field.

The transport equations for this model, as described by Charles Merkel in reference [7] are:

$$\rho\frac{\partial \kappa}{\partial t} + \rho u\frac{\partial \kappa}{\partial x} + \rho v\frac{\partial \kappa}{\partial y} + \rho w\frac{\partial \kappa}{\partial z} = +\frac{\partial}{\partial x}\left(\mu + \left[\frac{\mu_T}{Pr_k}\right]\frac{\partial \kappa}{\partial x}\right) + \frac{\partial}{\partial y}\left(\mu + \left[\frac{\mu_T}{Pr_k}\right]\frac{\partial \kappa}{\partial y}\right) + \frac{\partial}{\partial z}\left(\mu + \left[\frac{\mu_T}{Pr_k}\right]\frac{\partial \kappa}{\partial z}\right) + \mu_T\left(\frac{\partial u}{\partial x}\right)^2 + \mu_T\left(\frac{\partial v}{\partial y}\right)^2 + \mu_T\left(\frac{\partial w}{\partial z}\right)^2 - \varepsilon$$

and

$$\rho\frac{\partial \varepsilon}{\partial t} + \rho u\frac{\partial \varepsilon}{\partial x} + \rho v\frac{\partial \varepsilon}{\partial y} + \rho w\frac{\partial \varepsilon}{\partial z} = +\frac{\partial}{\partial x}\left(\mu + \left[\frac{\mu_T}{Pr_k}\right]\frac{\partial \varepsilon}{\partial x}\right) + \frac{\partial}{\partial y}\left(\mu + \left[\frac{\mu_T}{Pr_k}\right]\frac{\partial \varepsilon}{\partial y}\right) + \frac{\partial}{\partial z}\left(\mu + \left[\frac{\mu_T}{Pr_k}\right]\frac{\partial \varepsilon}{\partial z}\right) + \frac{C_{\varepsilon 1}\mu_T\varepsilon}{k}\left(\frac{\partial u}{\partial x}\right)^2 + \frac{C_{\varepsilon 1}\mu_T\varepsilon}{k}\left(\frac{\partial v}{\partial y}\right)^2 + \frac{C_{\varepsilon 1}\mu_T\varepsilon}{k}\left(\frac{\partial w}{\partial z}\right)^2 - \frac{C_{\varepsilon 2}\rho\varepsilon^2}{k}$$

where

Pr_k = turbulent Prandtl number (approximated as 1)

$k = \frac{1}{2} u_i u_i$

$C_{\varepsilon 1} = 1.0$

$C_{\varepsilon 2} = 1.2$

5. Convergence

When the problem is initialized, the values of each property in each cell are loaded into a matrix. By iterating the solution towards a smaller and smaller error value, the model reduces the residual values and undergoes a process known as convergence. Plots of the residuals inform the user of the quality of the solution. For steady state solutions, a residual convergence of three to five orders of magnitude indicates a good solution. For transient problems, the convergence is more likely to be one to three orders of magnitude. Plots of model convergences can be found in the appendix.

B. COMPUTATIONAL SETUP

1. Equipment

The computer resources utilized for the geometry generation and steady state flow modeling portion of this work were primarily a single desktop, Intel Xeon 5160 3GHz with 4 GB RAM running Windows Professional XP (SP2) 64 bit.

Mesh sensitivity and transient flow models were run on the King Lear super computer, which is an IBM P690 running AIX5.3 King Lear has 32 Processors, 132GB RAM and is connected via SCSI 320 lines to 1TB of Storage.

2. Software

The software package used to create a model of the geometry was Solidworks 2009 SP5.0 published by Dassault Systemes. Several features made this modeling package preferable to other available packages, specifically the ease of learning, the variety of geometric file export types and the customer support available.

The mesh creation, CFD solver and post processing were accomplished using Star CCM+ by CD-Adapco. This integrated package allowed the ready import of parasolid files and, once learned, allowed the rapid analysis of changes to the geometry. There were two versions of the software used during the course of the research because of an update release. The first version was 4.02.11 that was updated to 4.04.11

If there is to be further design work using these models, continued use of CCM is advisable, but not required.

C. TECHNICAL APPROACH

1. Overview

The overall approach to this project was to model an existing operational pulse detonation combustor with opposed multi-inlet design with sufficient fidelity to allow good predictions to be made of new design geometries with alternative features to meet new configuration needs. The issues involved in this endeavor mainly center on the unavailability of a software package and computational resources that can handle high speed, chemically reacting, unsteady flows around complex geometries at an acceptable resolution. The problem was therefore broken into several more tractable segments, namely:

- Correct grid resolution (mesh sensitivity)
- Steady state flow structure visualization and geometry refinement to avoid recirculation
- Transient fuel dispersion modeling
- Geometry refinement for fuel dispersion

To perform a mesh sensitivity analysis a series of increasingly refined mesh models were used and the computational results compared with empirically measured variables such as the pressure loss across the detonation tube obstacle field. The model pressure differentials were then compared with the measured value at the same mass flow rate as a percentage error and plotted against the base mesh size. Once the model demonstrated a favorable comparison to empirical pressure drop data, the grid sizing on the model could be adjusted to quantify the variance of pressure drop error (model accuracy) with cell size (computational complexity). By comparing these values over a range of mesh densities a model complexity could be intelligently chosen to maximize accuracy without loading the computational resources unnecessarily.

After determining an acceptable mesh size the research focused on the steady flow simulation of a non-reacting gas through the proposed single inlet geometry with very slight modifications to the igniter and shroud to accommodate those changes. This series of model refinements comprised the bulk of the research and included, as a start, determining the effect of inlet angle on recirculating flow structures surrounding the igniter shroud. Once it had been determined that using a shallow inlet angle alone would not eliminate recirculation zones without making the angle excessively shallow (smaller than 30 degrees) a different approach had to be developed to accomplish this goal. Shortening the region upstream of the dump inlet had positive effects but also could not eliminate the recirculation zones in the vicinity of the extreme upstream portion of the head-end opposite the dump plane. The semi-headless design may have an acceptably small magnitude of recirculation but, since the area of recirculation serves no other purpose, eliminating it and progressing to a fully headless design satisfied the design objective more fully without adversely affecting manufacturability.

Once the recirculation issue was addressed in steady state, the final challenge was to ensure adequate fuel dispersion in the transit from the injector to the igniter. For this investigation the final 30 degree headless design was modeled with transient flow and examined for fuel-air concentration at various points along the flow path at specific time intervals.

2. Modeler and Model

a. Modeling

The modeling process itself consists of forming parts and then fitting them into assemblies. The parts were the detonation tube body, the igniter shroud, and the igniter. Fasteners were not modeled.

The main body consists of a constant cross section diameter along a pre-defined path that was modified by adding receptacles for the igniter shroud, igniter and flanges. The igniter shroud is a thin walled tube perforated by symmetric holes. The igniter is a stepped concentric right circular cylinder, as shown in Figure 5.

The assembly process places the shroud inside the detonation tube cavity and the igniter inside the shroud. All assembly fits were fixed such that no degrees of freedom remained between the parts. Once the assembly was complete the geometry was saved as either a parasolid (.x_t) or Solidworks assembly (.ASM) file.

Successive design typologies led to shorter and shorter head lengths until the eventual development of the headless design as well as the switch from long ceramic rod igniters to spark plug style igniters to remove the concern regarding cross flow stresses. With the head shortened to the rear plane of the inlet tube the semi-headless design was modeled, which significantly reduced recirculation in all areas except the zone adjacent to the head wall opposite the dump inlet. This persistent area of recirculation could only be swept out of the igniter region by making it part of the primary flow path, hence the development of the headless geometry.

b. Grid (or Mesh)

Once the geometric model was completed the interior volume had to be defined and meshed appropriately for computation. The STAR CCM program was utilized for gridding as well as solving and post processing. The four program selections used in meshing for these models were the inclusion of the surface remesher and surface wrapper and the selection of cell shape (polyhedral) and inclusion of prism layers (near wall thin boundary layer cells).

The surface remesher is used to conform an existing surface in order to improve the overall quality of the surface and optimize it for the volume mesh models. The remeshing is primarily based on a target edge length supplied by the user and can also include feature refinement based on curvature and surface proximity. Localized refinement based on boundaries can also be included. In addition to improving the surface for the volume meshers it aids the subsurface generator when the prism mesher option is selected. This allows a custom mesh to be generated by the user.

The surface wrapper is the tool used to topologically differentiate between the inside and outside of surfaces. Since the representation of a complex geometry is digital there are likely to be, at some level, gaps in the continuity of the solid. The surface

wrapper size selection determines what the program will consider a hole. A fully enclosed surface has no ‘leaks’ through which fluids might transfer from one volume into another. The size selection acts as a ‘go, no-go’ test for each potential gap. If the wrapper tool is sufficiently sized, intentional gaps can be captured in the model without including micro gaps caused by computer round off error or program interpretation errors.

Basic shape selection for mesh geometries has traditionally been tetrahedral in many codes, and CCM supports that, but their manufacturer’s recommendation is that polyhedral meshes be used. This reduces the effective perimeter for a given enclosed volume (honeycomb conjecture) [8]. By minimizing the number of faces containing any given volume the number of face calculations required to resolve properties within that volume is similarly minimized. Additionally, the use of polyhedral meshes links each specific cell to more (on average) cells than tetragonal meshing does. This increases the interdependence of cells on their neighbors, which more appropriately reflects the behavior of real fluids. The final parameter is prism layer inclusion near wall boundaries. This is important for viscous flow analysis due to the behavioral differences between fluid particles near walls and those in the free stream (outside the boundary layer). Traditional boundary layer sub-gridding divides the near-wall region into many parallel cells, each one slightly thicker than then it’s neighbor cell immediately closer to the wall (recommended growth rates are on the order of 1.2 times). This code divides the sub-grid into fewer sections with higher growth rates to cover similar boundary layer thicknesses to avoid the large aspect ratios that would result from extremely thin cross sectional profiles and the computational problems inherent in those aspect ratios.

There are many options for generating volume meshes, many of which will give adequate results and none of which is optimum in all cases. For simplicity of operation and to preserve the validity of comparison between models a single mesh format was chosen.

Fundamentally, a valid mesh is one that allows for the simulation to be initialized and iterate so that a solution is achieved. An invalid mesh is typically one for which no solution can be obtained or cannot even be initialized. As an example of the latter situation, a mesh that contains a negative volume cell would be considered invalid.

However, the determination of whether a mesh is valid or not is sometimes dependant on the underlying mesh quality and/or the physics selected to be used for the mesh. For example, the inclusion of cells with high concave angles would not normally cause a problem for basic flows but in cases with high gradients or more complex physics, the mesh might become invalid and not provide a solution anymore. Other factors that can affect whether a mesh is valid include:

- choice of solver (coupled or segregated)
- under-relaxation or Courant number specification; and
- discretization scheme used

The approach used to define a CFD analysis is also important. For example, adding the physical models in one by one, iterating and restarting for each might lead to a valid solution. However, adding in all the physical models at once and attempting to run the simulation might cause the solution to diverge for a given mesh. The mesh validity checks that are performed in STAR-CCM+ are:

- Unclosed cells
- Invalid cell/vertex references
- Zero area faces
- Zero or negative cell volumes

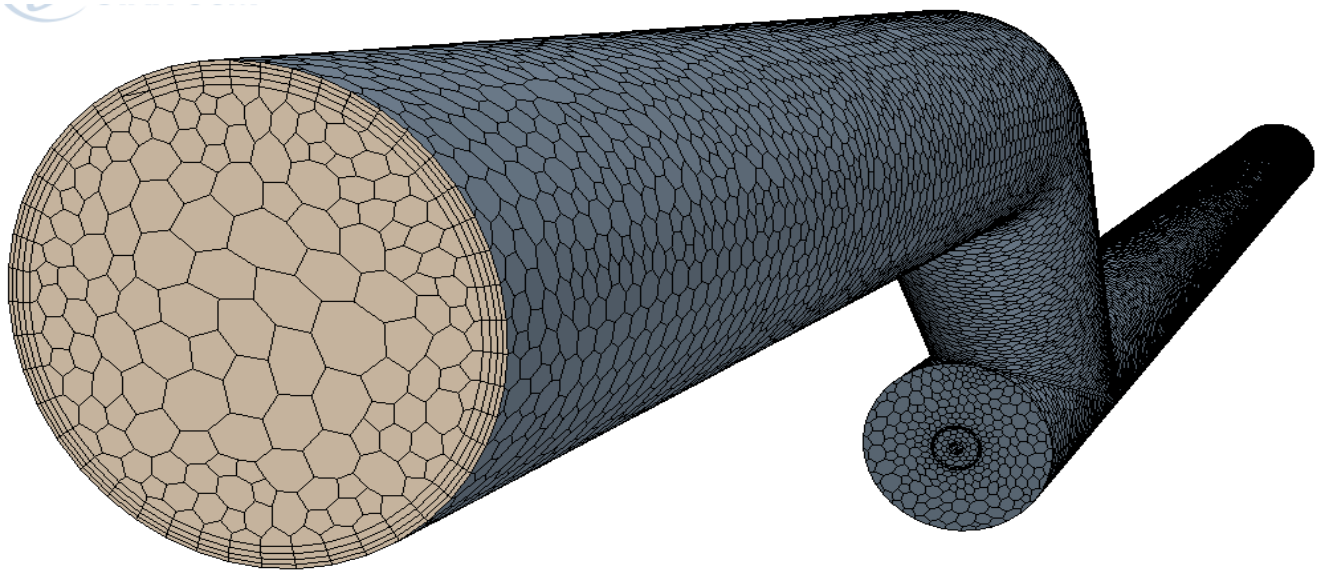

Figure 15. Typical mesh of one branch downstream of the injector

The light colored circular region near the left side of Figure 15 is where the fluid enters this section of the model. Note the four prism layers of increasing width near the outer wall. There is a mesh refinement around the section of particular interest (igniter and shroud) that can be better seen in Figure 16.

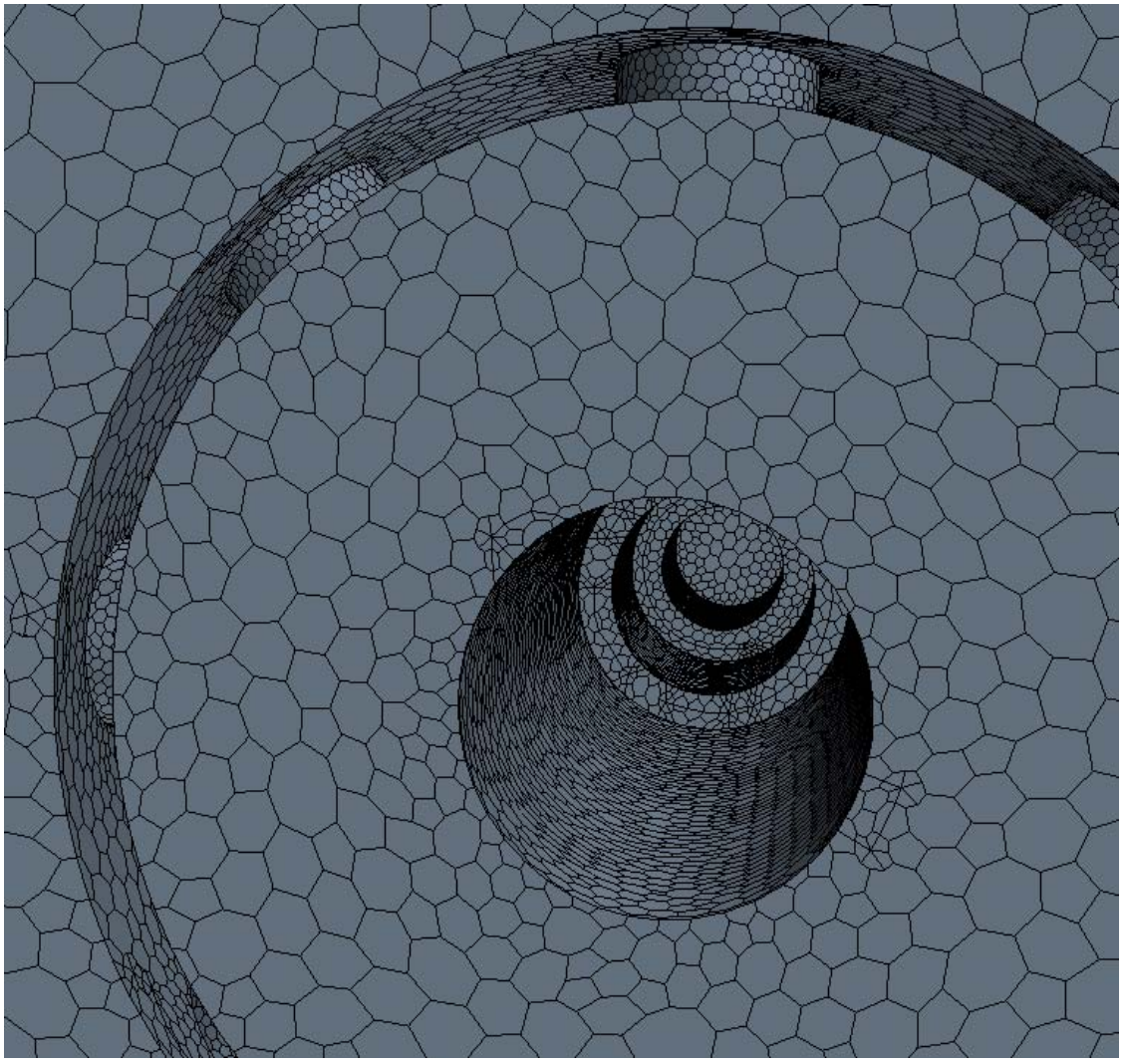

Figure 16. Rear view of mesh (Igniter detail)

This view (Figure 16) is taken from the surface of the head end looking into the flow volume. The interior stepped space is where the igniter would sit. The annular gap is where the igniter shroud is located and the radial columns are the holes through it. No prism layers are visible in this view because they would be on the far side of this geometry's envelope.

Some items to note:

The semi-regular shape of the cells is a result of random elements in the best-fit algorithm propagating from a mesh seed inside the volume of interest. Also, the

size of the cells near the boundaries is smaller than the cell size near the free stream. This helps resolve important features around boundary geometry without excessively loading the processor with additional cells.

c. Solver

The physics solver contained in STAR CCM has many options. The ones chosen for this family of solutions are:

Stationary – The structure (wall geometry) is rigidly fixed in space

Steady state – Fluid flow is time independent. A transient model was also run on an Implicit Unsteady solver to establish sufficiency of fuel dispersion.

Ideal gas (air) – The physical properties of air are used and it is treated as complying with the ideal gas law (PV=RT). Specific properties for these models were:

Table 2. Air properties

Dynamic Viscosity	1.85508E-5 Pa-s
Molecular Weight	28.9664 g/mol
Specific Heat (Cp)	1003.62 J/kg-K
Thermal Conductivity	0.0260305 W/m-K
Turbulent Prandtl Number	0.9

Ideal Gas (ethylene) – To determine the concentration of fuel in the transient models a mixed gas flow (air and ethylene) was incorporated. The ethylene properties used in these models were:

Table 3. Ethylene properties

Dynamic Viscosity	1.03406E-5 Pa-s
Molecular Weight	28.05 g/mol
Specific Heat (Cp)	1541.338 J/kg-K
Thermal Conductivity	0.0196139 W/m-K
Turbulent Prandtl Number	0.9

Segregated Flow – The Segregated Flow model solves the flow equations (one for each component of velocity, and one for pressure) in a segregated, or uncoupled, manner. The linkage between the momentum and continuity equations is achieved with a predictor-corrector approach. The complete formulation can be described as using a collocated variable arrangement (as opposed to staggered) and a Rhie-and-Chow-type pressure-velocity coupling combined with a SIMPLE-type algorithm. These models were run using a 2nd order upwind convection scheme.

Turbulent (κ-ε model) – A standard κ-ε turbulence model is a two-equation model in which transport equations are solved for the turbulent kinetic energy κ and its dissipation rate ε. Various forms of the κ-ε model have been in use for several decades, and it has become the most widely used model for industrial applications. The Standard K-Epsilon Model is a de facto standard version of the two-equation model. The transport equations are of the form suggested by Jones and Launder [9], with coefficients suggested by Launder and Sharma [10].

d. Post Processing

Within the CCM suite the data is converted, via user input, to specific scenes. These are generally views of a specific parameter (e.g., pressure, velocity) represented by either a vector or a scalar. Display of scalars is in the form of a colored two-dimensional map, while vectors are viewed in pseudo three-dimensions as colored and scaled arrows.

More complex scenes can trace streamlines along the flow path and display the paths of imaginary particles within the flow field. The animation of these scenes provides the viewer with a good visualization of dynamic states as in the variation of velocity along a streamline.

Of primary interest to this study was the phenomenon of recirculation zones surrounding the igniter and shroud. These bubbles were visualized using pressure and vorticity plots as well as streamline traces of velocity.

D. DATA ANALYSIS (EMPIRICAL VALIDATION)

The mesh parameters were validated by comparing the computer model prediction of pressure drop across the detonation initiation ramps to the experimental rig measurements of the same configuration. The experiment was run as part of a cold flow test focused on ramp properties and was included here to prevent the duplication of effort and additional rig wear. This validation compared pressures by measuring each models output at an upstream and downstream position, taking the difference, comparing that difference to the actual pressure drop and expressing the error as a relative percentage. As can be seen in the table and figure below the relative error is very large at a 10 mm cell size and narrows rapidly to within a few percent by 3.75mm. With error values in this range, the accuracy of empirical pressure transducer measurements, ability to accurately measure pressure tap location and to localize specific cell data start to affect the prediction of the expected error values. The models were run with a 2.5 mm target cell size and expected errors are well within the range of acceptable values for experimental design work.

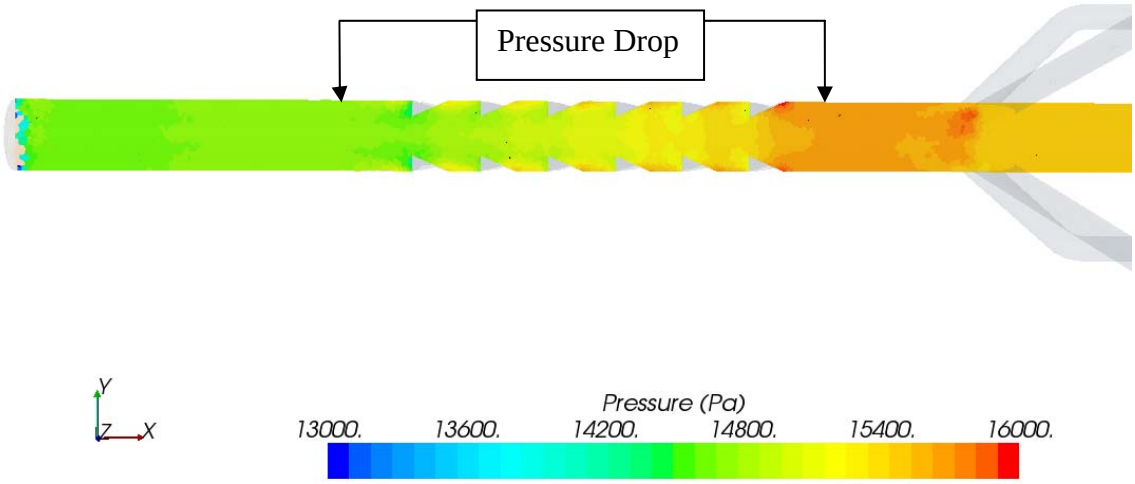

Figure 17. Longitudinal Pressure Distribution (Current Geometry)

Figure 17 displays pressure variation across the detonation obstacle ramp arrangement. This is the measurement utilized to validate the model predictions against the measurements taken on the experimental rig.

Table 4. Mesh Size and Pressure Drop Comparison Data

Faces (#)	Vertices (#)	Cells (#)	Abs Tgt. Size (mm)	US-P (Pa)	DS-P (Pa)	Del P (Pa)	Del P error (Pa)	Rel Err (%)
4398092	3476539	776776	10	2805	2785	20	-3282	99.39
5627248	4478876	976995	8.75	2900	79	2821	-481	14.56
3956999	3122123	893658	7.5	4650	1280	3370	68	2.06
5870081	4672031	1019297	6.25	3270	-60	3330	28	0.85
4480665	3547176	1111816	5	2980	105	2875	-427	12.93
6115416	4882938	1053618	3.75	3520	100	3420	118	3.57
8552575	6915690	1425329	2.5	3450	100	3350	48	1.45

In Table 4, all pressures are measured in Pascal with an atmospheric reference (Gauge Pressure). The Absolute target size is in millimeters.

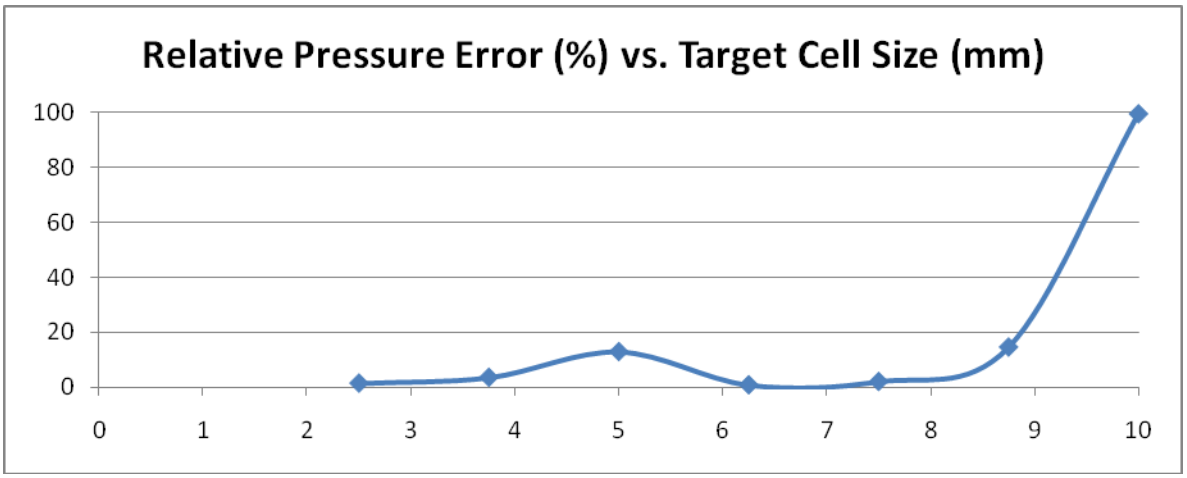

Figure 18. Plot of Relative Pressure Error vs. Computational Cell Size

As shown in Figure 18, the early low error values associated with the 7.5mm and 6.75mm cell sizes would have been acceptable had the 5mm cell error not risen so high (above 5%). Though a specific cause for this rise in error at the 5mm cell sized could not be identified, it is suspected that the apparent large error is a coincidence of the next two larger cell sizes having fortuitously accurate results.

Within the scenes produced from the models, there is often additional data presented that obscures the parameter of interest. For that reason, many figures have been adjusted to show only parameters within a particular range of values. The data is still retained in the model output and is available for use by follow on researchers. Two specific examples of this are the display of only low velocities in the recirculation regions of the dump angle variance experiment for visual clarity and the narrow scale of pressures displayed in the upstream and downstream pressure cross sections to make the output more distinguishable.

The results are consistent with similar research on Ramjet combustor pressure losses by Braclay [11].

THIS PAGE INTENTIONALLY LEFT BLANK

III. RESULTS

The models generated allowed for visualization of internal flow structures, which allowed design decisions to be made regarding appropriate geometry changes. The two major contributors to recirculating behavior in the igniter region were dump angle and head depth, whereas the driving parameter for fuel dispersion was induced swirl.

A. DUMP ANGLE VARIATION

The investigation into the variation of characteristics of the recirculation zones surrounding the igniter and shroud with entrance angle determined that there was an increase in recirculation intensity with larger dump angles. The following three figures display traces of streamlines through flow fields generated by varying the dump angle. For clarity, all velocity vectors of greater than 40 m/s have been eliminated and the angle at which the figure view is displayed is varied to best represent the shape and size of a three dimensional phenomenon in a two dimensional format. In these figures, the primary flow is composed of the much more abundant red and yellow streamlines that, in an unedited picture, completely fill the central section and often interfere with the clear viewing of the recirculation.

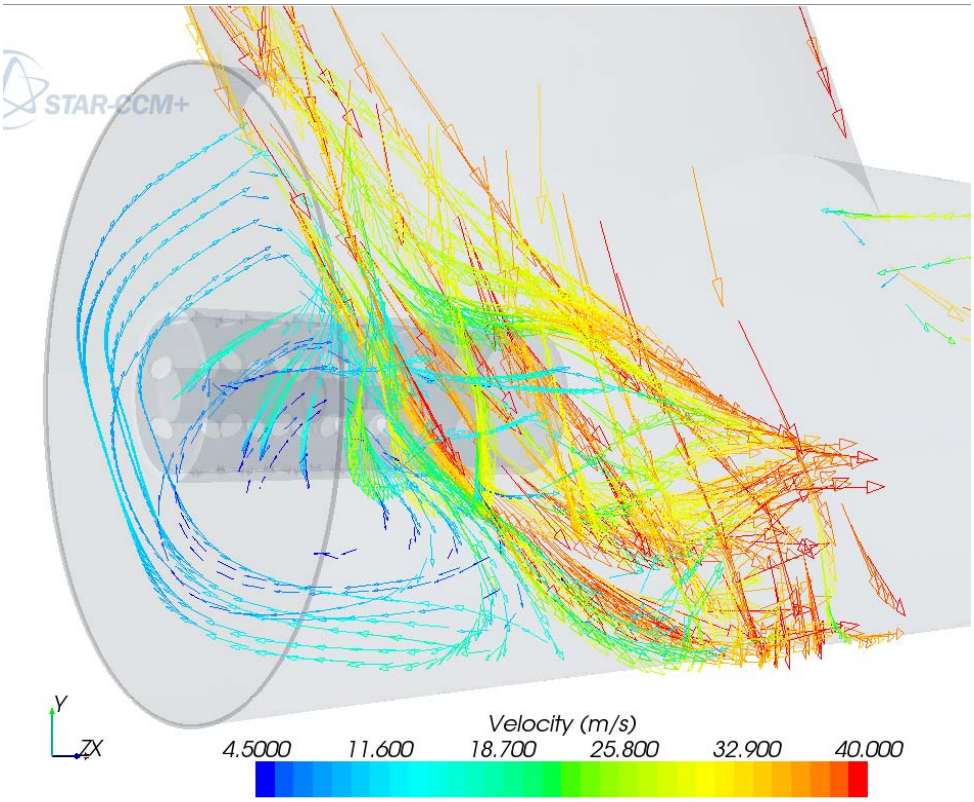

Figure 19. Recirculation for 60 degree inlet angle

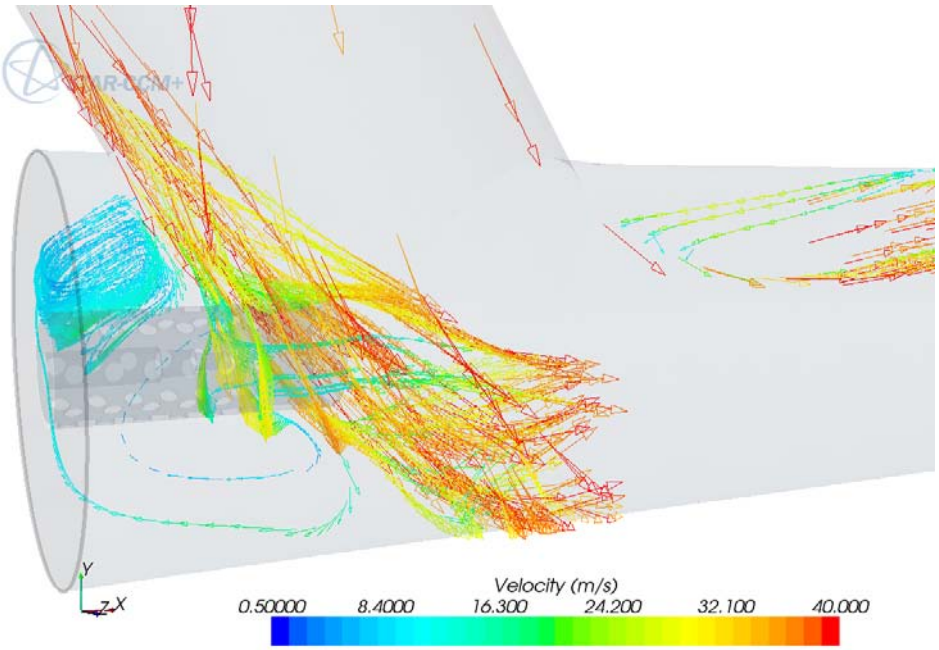

Figure 20. Recirculation for 45 degree inlet angle

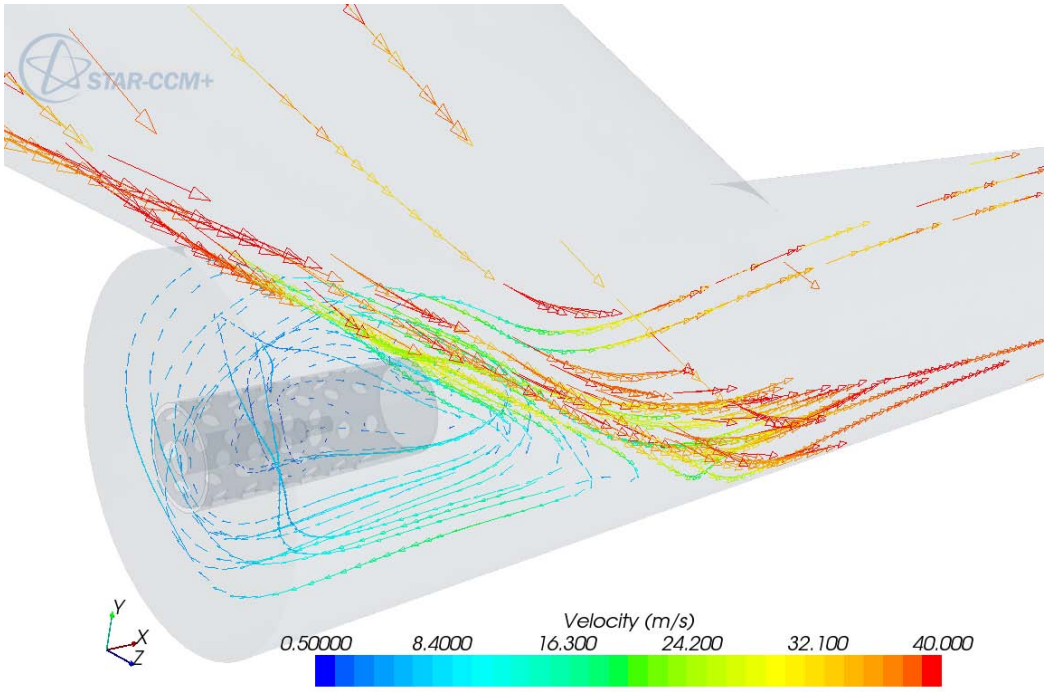

Figure 21. Recirculation for 30 degree inlet angle

Note that even with the reduction of dump angle a recirculation zone persists in the head-end region surrounding the igniter shroud. For completeness and a sense of scale, the following longitudinal cross section view displays a close up view of the dump and head sections of the 30-degree model.

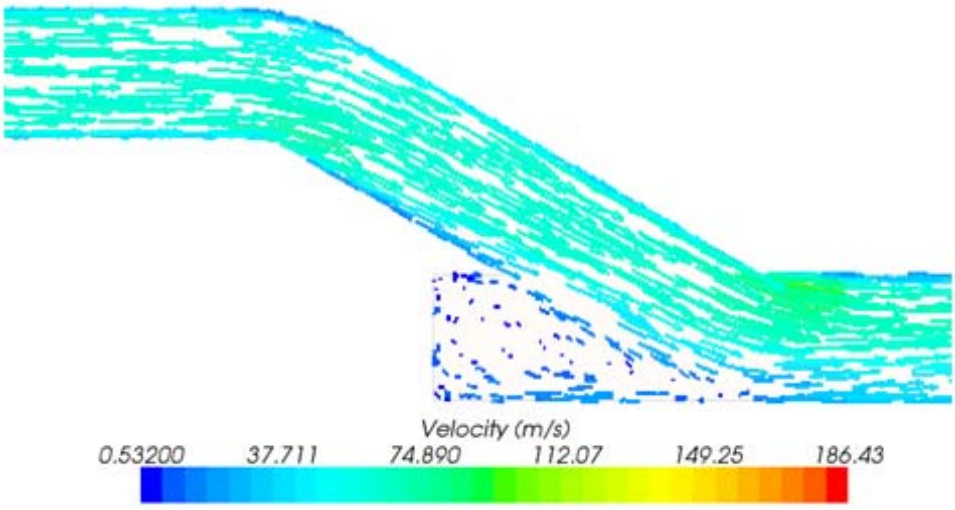

Figure 22. Longitudinal section velocity distribution (30 degree dump angle)

The flow patterns in the figures 19 through 21 contain strong elements resembling the backstep recirculation (Figure 13) and the crossflow cylinder recirculation (Figure 12). Higher dump angles also appear to involve some of the characteristics of the bent pipe flow pattern when viewed from the appropriate angle. Visualization of all of these characteristics is facilitated by motion video of the streamlines, as provided in Appendix C – multimedia DVD #1. For viewing from different angles, the appropriate .sim file will have to be opened and the associated scene regenerated.

B. HEAD DEPTH

After visualizing these flows, the igniter/shroud attachment geometry was redesigned to exclude the head region upstream of the inlet. Shortening the head reduced the amount of recirculation present, but could not eliminate the persistent recirculation in the region directly opposite the dump plane. Since the original model had no such region a meaningful comparison of the ignition characteristics between the model geometry and the operating geometry could not necessarily be drawn. It was decided to further refine the model geometry to entirely eliminate the secluded area to eliminate the recirculation. Eliminating the head-end region required that the igniter attachment and support method be reexamined, since there was no longer a flat plate on which to mount the components. A coaxial support tube that penetrated the rear wall at an angle and was sturdy enough to support the ignition assembly was developed and used in the headless design.

C. TRANSIENT ANALYSIS OF FUEL DISTRIBUTION

Upon investigating the fuel distribution characteristics of the simple coaxial injector model, it was discovered that the bulk of the fuel was not well mixed in the longitudinal plane. Of particular concern was the very lean condition next to the igniter.

As with Danaher's [12] work on PDEs the model used ethylene as a fuel.

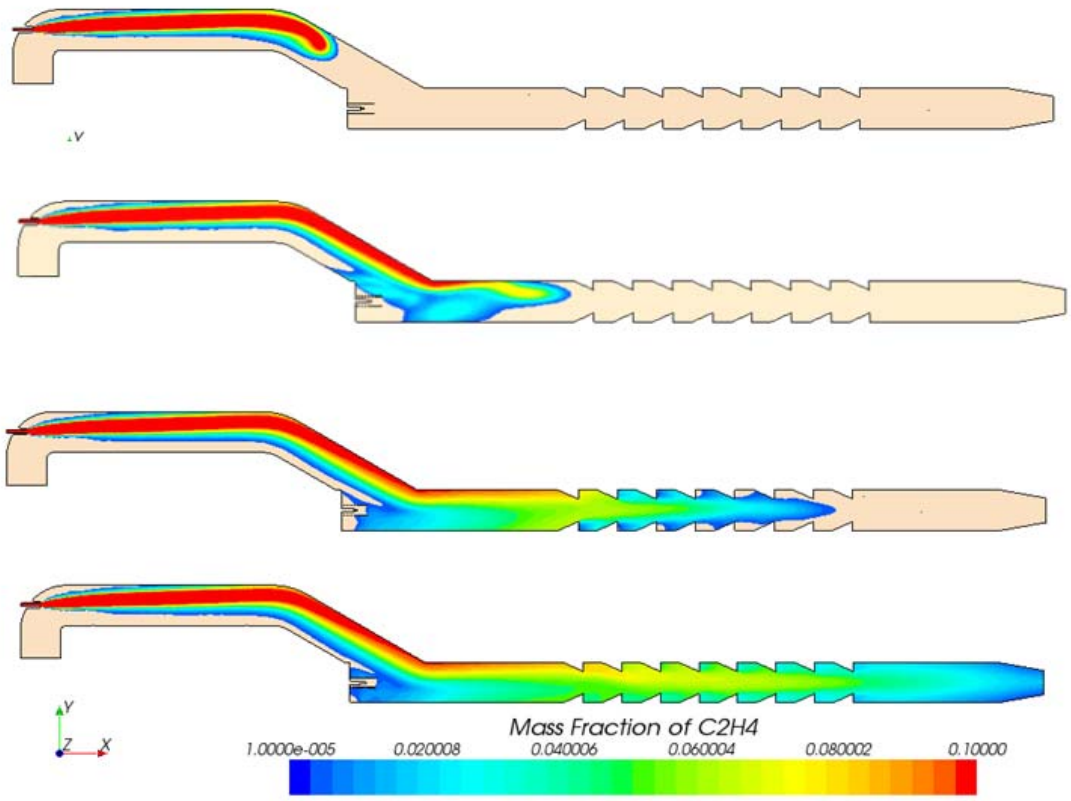

Figure 23. Fuel Concentration Distribution Progression (Longitudinal Section)

Figure 23 depicts the evolution of the fuel dispersion after the initiation of injection. The tan areas represent the absence of fuel. Figure 23 allows the viewer to visualize the leading edge of the fuel slug through time. Note that as the slug of fuel progresses along the detonation tube the concentration is highly stratified, with the fuel rich regions concentrated along the upper wall. The detonation inducing ramps do appear to have a mild homogenizing effect on the mixture, but the area adjacent to the igniter and shroud is extremely lean along the centerline. This overly lean condition is not acceptable in a reliable design.

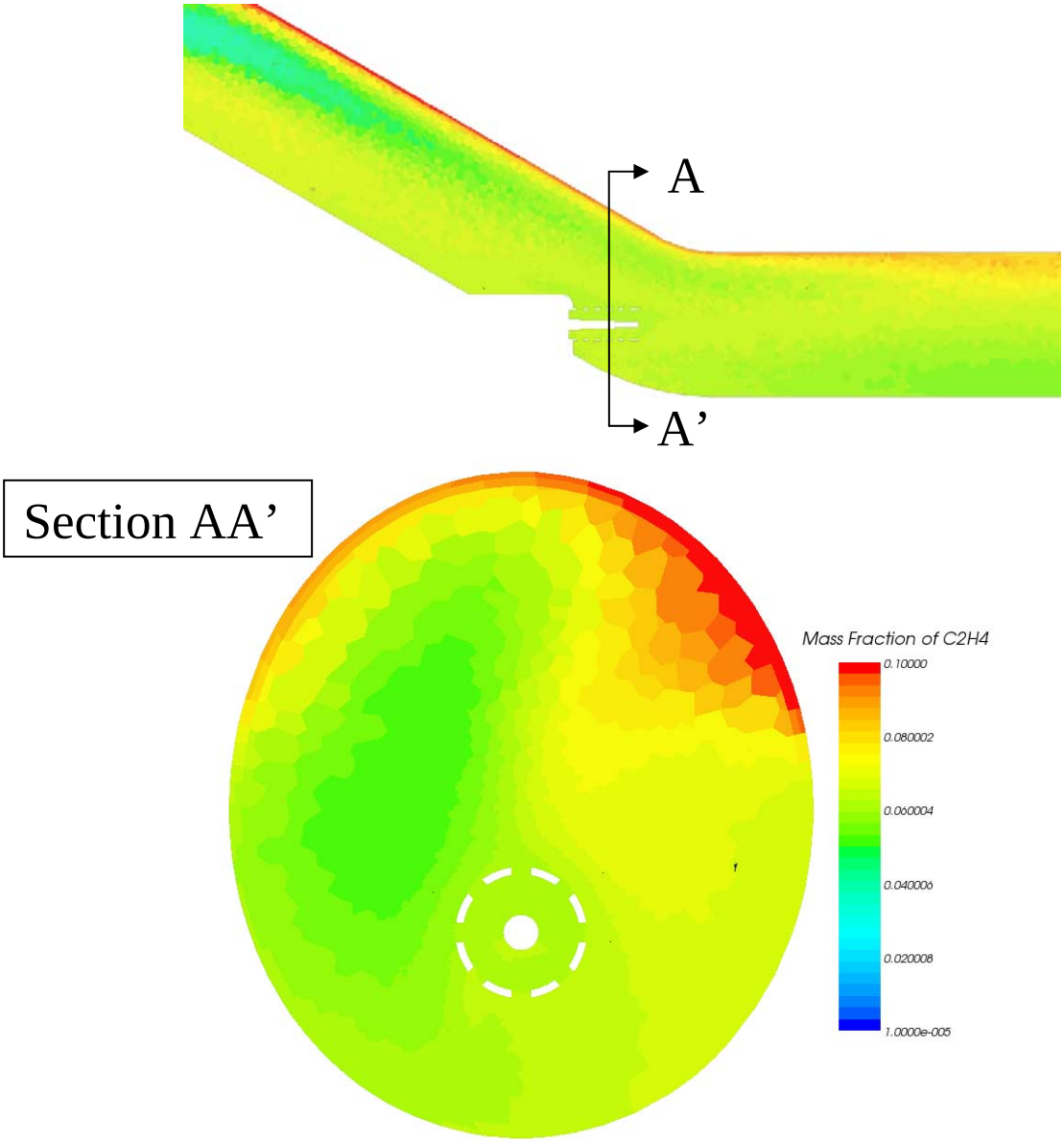

Figure 24. Fuel Concentration Distribution (Igniter Cross Section, 15ms)

This detailed cross section taken at the plane of the igniter displays the concentration of combustible gas mixture well away from the igniter. This, in conjunction with the longitudinal view indicating an overly lean mixture in the entire region surrounding the igniter contraindicates use of the simple coaxial injector with a semi-headless design.

1. Swirl

Due to the large fuel concentration gradient in the inlet arm, a modified fuel injector rig was designed, generated and applied to a headless geometry for transient fuel dispersal modeling. The modification introduced four radial fins canted to induce right-handed swirl along the axis of flow. The geometry can be seen below in Figure 25.

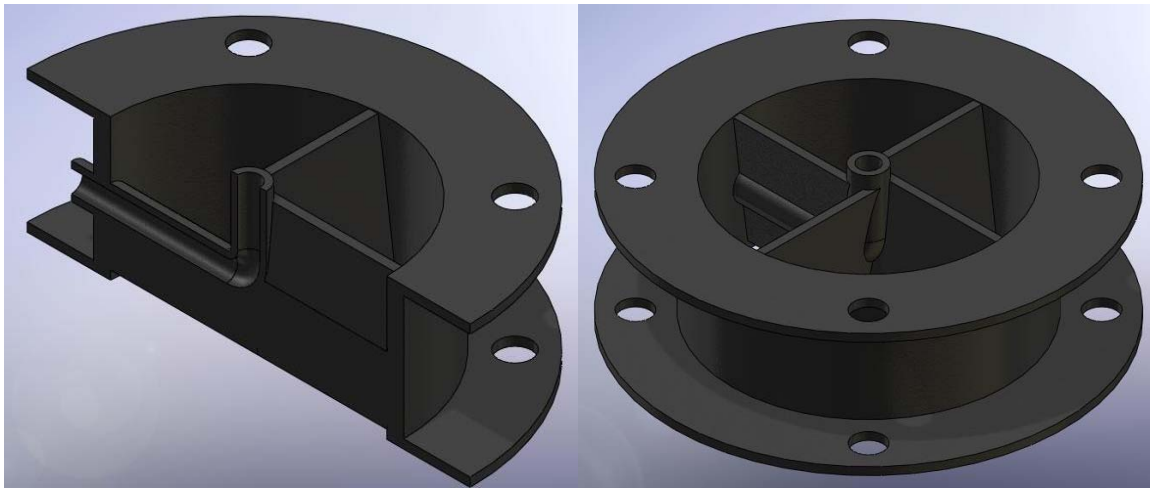

Figure 25. Swirl Generating Fuel Injector (Section and Trimetric views)

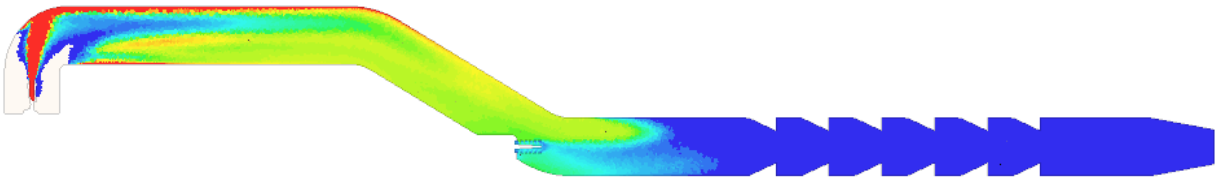

Figure 26. Fuel Concentration Distribution (Longitudinal Section, final geometry)

As can be seen on the mid-plane section in Figure 26, the longitudinal swirl results in much more rapid fuel dispersion. By the time the first fuel particles have reached the igniter section, the fuel-air mixture is mostly homogenized. This will result in a far superior condition for ignition than resulted from using the coaxial injector.

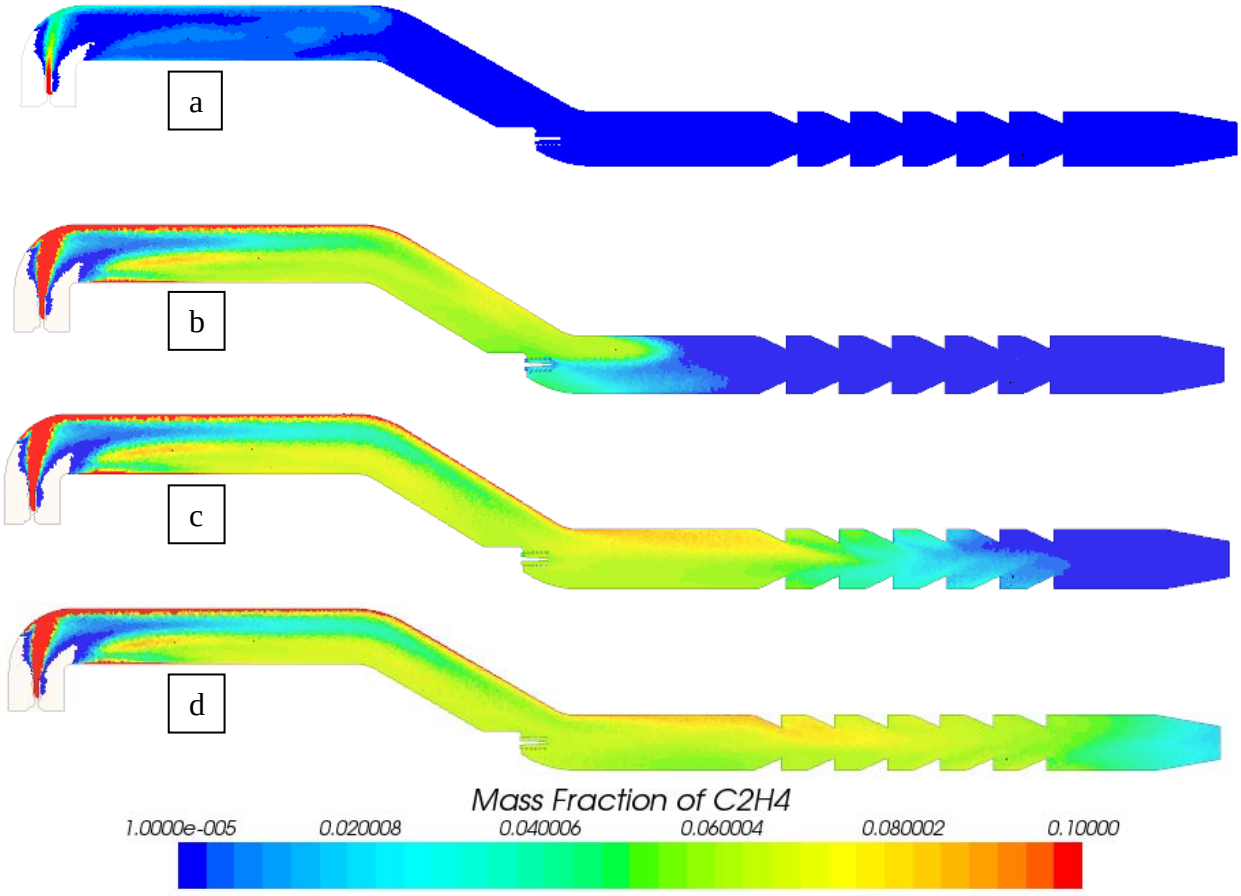

Figure 27. Fuel Concentration Distribution (a:5ms, b:10ms, c15ms: and d:20ms)

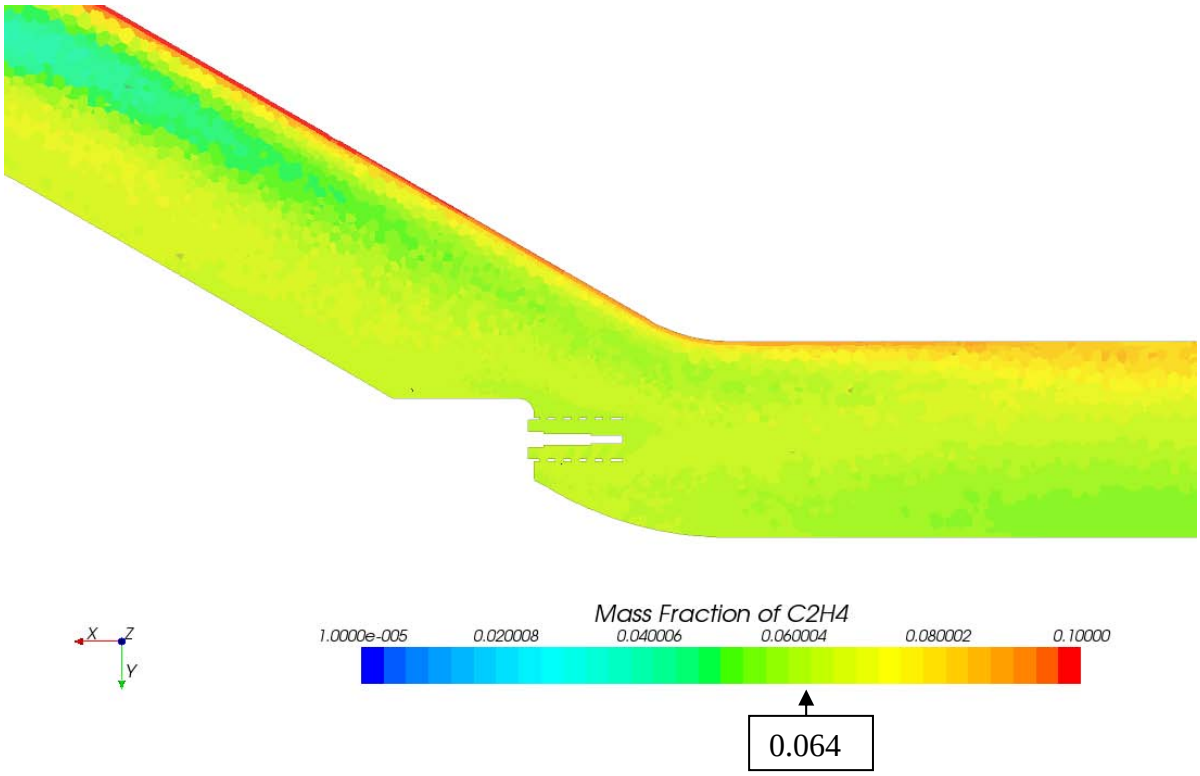

Figure 28. Fuel Concentration Distribution (15 ms, detail view)

The headless design combined with the induced swirl injector smoothes out the stratifications in the fuel concentration. It can be seen in Figure 27 that by the time the fuel front passes the igniter it is fairly well mixed in the center plane. It is also at approximately the stoichiometric ratio of 6.4% (by mass) for a large portion of the surrounding volume.

The ignition will trigger when the fuel front has moved to the end of the detonation tube and the rearmost-fueled region is approaching the igniter (Back end ignition). The mixture should be even more homogenized at that point as shown in Figure 27 d.

2. Injector Location

Due to the turbulent nature of the flow and the normal diffusion characteristics of the fuel, the longer the flow path between the injector and the igniter the more homogenized the fuel-air mixture will be at the igniter plane.

THIS PAGE INTENTIONALLY LEFT BLANK

IV. SUMMARY

A. CONCLUSIONS

The models run for this thesis produced results that are fairly easily visualized and conform to the expectations developed by observers of fluid motion. No model predicted any flow pattern or concentration that was counter-intuitive once the input assumptions and scales of individual phenomena were taken into account.

A headless design combined with some form of fuel mixing device produced the best results for a robust system. Similar geometries should be used in the final design.

It will be possible to effectively employ single side-dumped combustors for pulse detonation systems. Both the recirculation and fuel mixing issues are readily addressed by geometry changes.

B. RESEARCH AND DESIGN RECOMMENDATIONS

Placement, orientation and porosity of the igniter shroud will need to be examined to ensure that sufficient mixed fuel flow enters the enclosed region. Similarly, the angle at which the porosity holes penetrate the shroud is perfectly radial in the current geometry. Changing those porosity hole sizes and angles may allow finer control of the flow inside the shroud.

The support collar for the igniter and shroud in the headless design uses a simple circular cross section. There may be pressure loss advantages to changing to a more streamlined profile.

The three-tube rig geometry has the dump tube cant inward (towards the center of the triangle formed by the three detonation tubes) for ease of construction and simplicity. By rotating the cant so that it is more circumferential than radial a larger moment arm could be developed as well as clearing the interior of the space for other hardware such as booster engines. This should be considered for the final design.

THIS PAGE INTENTIONALLY LEFT BLANK

LIST OF REFERENCES

[1] Kashif Kahn, "The Specific Impulse of Various Hydrocarbon Fuelled Jet Engines." Available at: http://en.wikipedia.org/wiki/Specific_impulse [Accessed: SEP 10, 2009].

[2] W. H. Heiser and D. T. Pratt, "Thermodynamic cycle analysis of pulse detonation engines," *Journal of Propulsion and Power*, vol. 18, no. 1, pp. 68–76, FEB 2002.

[3] K. Kuo, *Principles of Combustion*. New York: John Wiley and Sons, 1986.

[4] R. Yen and T. Ko, "Effects of single inlet angle in a three-dimensional side-dump combustor," *Journal of Propulsion and Power*, vol. 19, No. 5, pp. 686–693, OCT 1993.

[5] N. S. Nosseir and S. Behar, "Characteristics of Jet Impingement in a Side-Dump Combustor," American Institute of Aeronautics and Astronautics, vol 24, pp. 1752–1757, NOV 1986.

[6] M. W. Deppe, "Combustion Efficiency in a Dual-Inlet Side-Dump Ramjet Combustor," M.S. thesis, Naval Postgraduate School, Monterey CA, USA, 1994.

[7] C. Merkel, "Computational Fluid Dynamics of Inviscid and High Reynolds Number Flows," Unpublished Notes.

[8] T. Hales, "The Honeycomb Conjecture," The Honeycomb Conjecture, JUL 99. Available: http://xxx.lanl.gov/abs/math.MG/9906042 [Accessed: SEP. 10, 2009].

[9] W.P. Jones and B.E. Launder, "The prediction of laminarization with a two-equation model of turbulence," *International Journal of Heat and Mass Transfer*, vol. 15, pp. 301–314, Feb 1972.

[10] B.E. Launder and Sharma, "Application of the energy-dissipation model of turbulence to the calculation of flow near a spinning disc," *Letters in Heat and Mass Transfer*, vol. 1, no. 2, pp. 131–138, 1974.

[11] L.P. Barclay, "Pressure Losses in Simple Dump Combustors," Air Force Aero Propulsion Lab, Wright-Patterson AFB, OH, USA, Tech. Rep. AD0906402, OCT 1972.

[12] T. Danaher, "Characterization of Ethylene/JP-10 Fuel Injection Profiles for a Valveless Pulse Detonation Engine," M.S. thesis, Naval Postgraduate School, Monterey CA, USA, 2007.

THIS PAGE INTENTIONALLY LEFT BLANK

APPENDIX A

(RESIDUAL PLOTS OF REPRESENTATIVE CONVERGED MODELS)

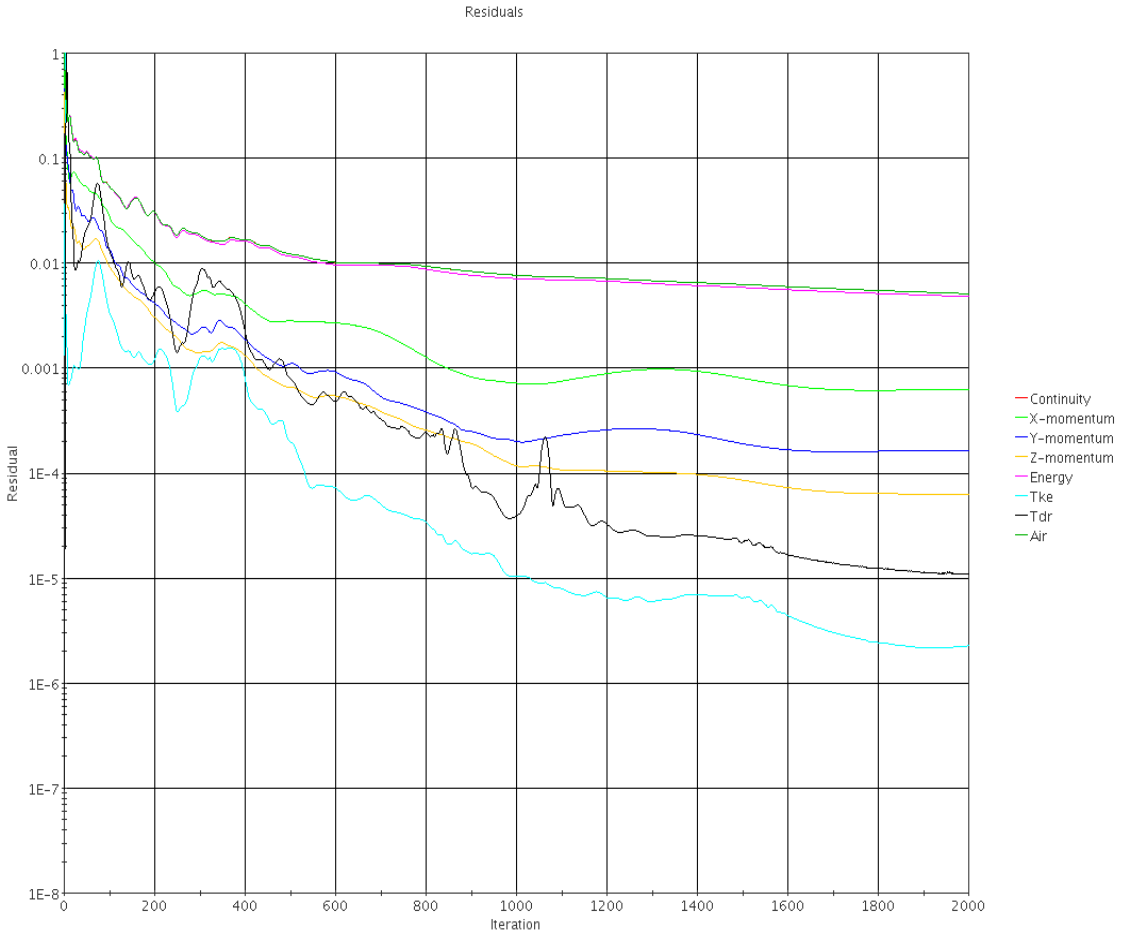

Figure 29. Convergence Residuals (current geometry, static starting solution)

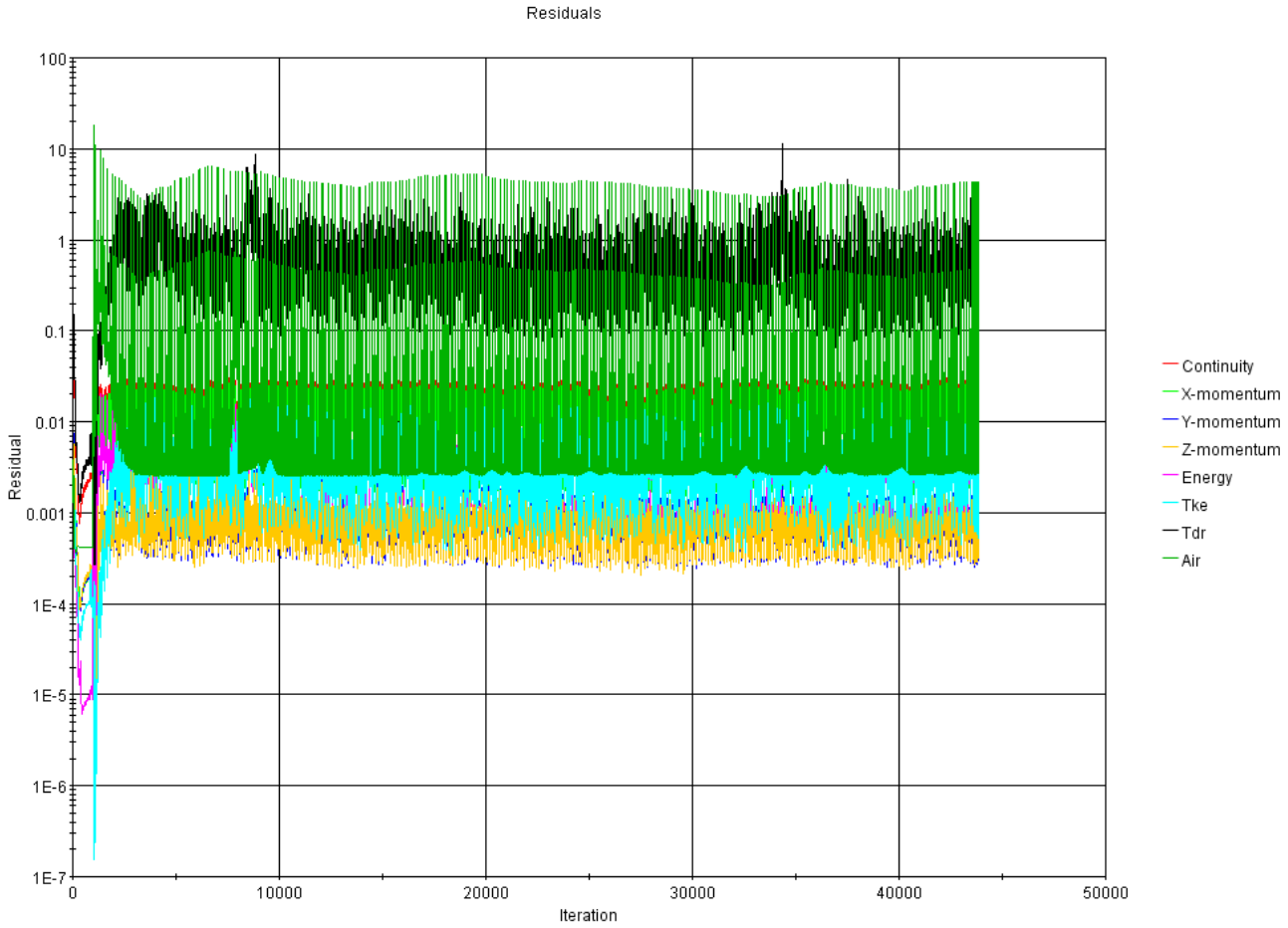

Figure 30. Convergence Residuals (transient solution @ 43000 iterations)

APPENDIX B

(FINAL DESIGN PLANS)

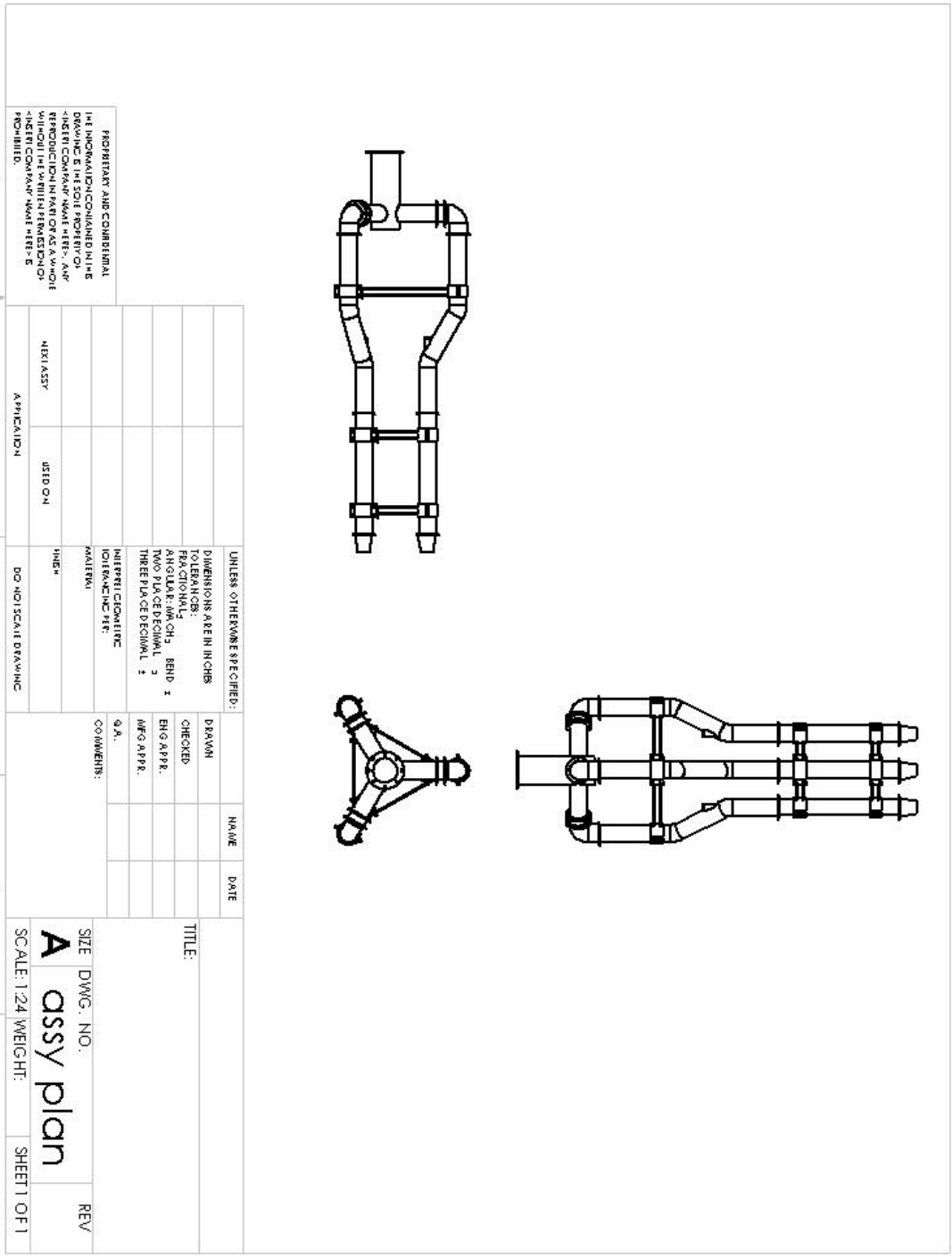

Figure 31. Schematic (Three-Tube-Rig)

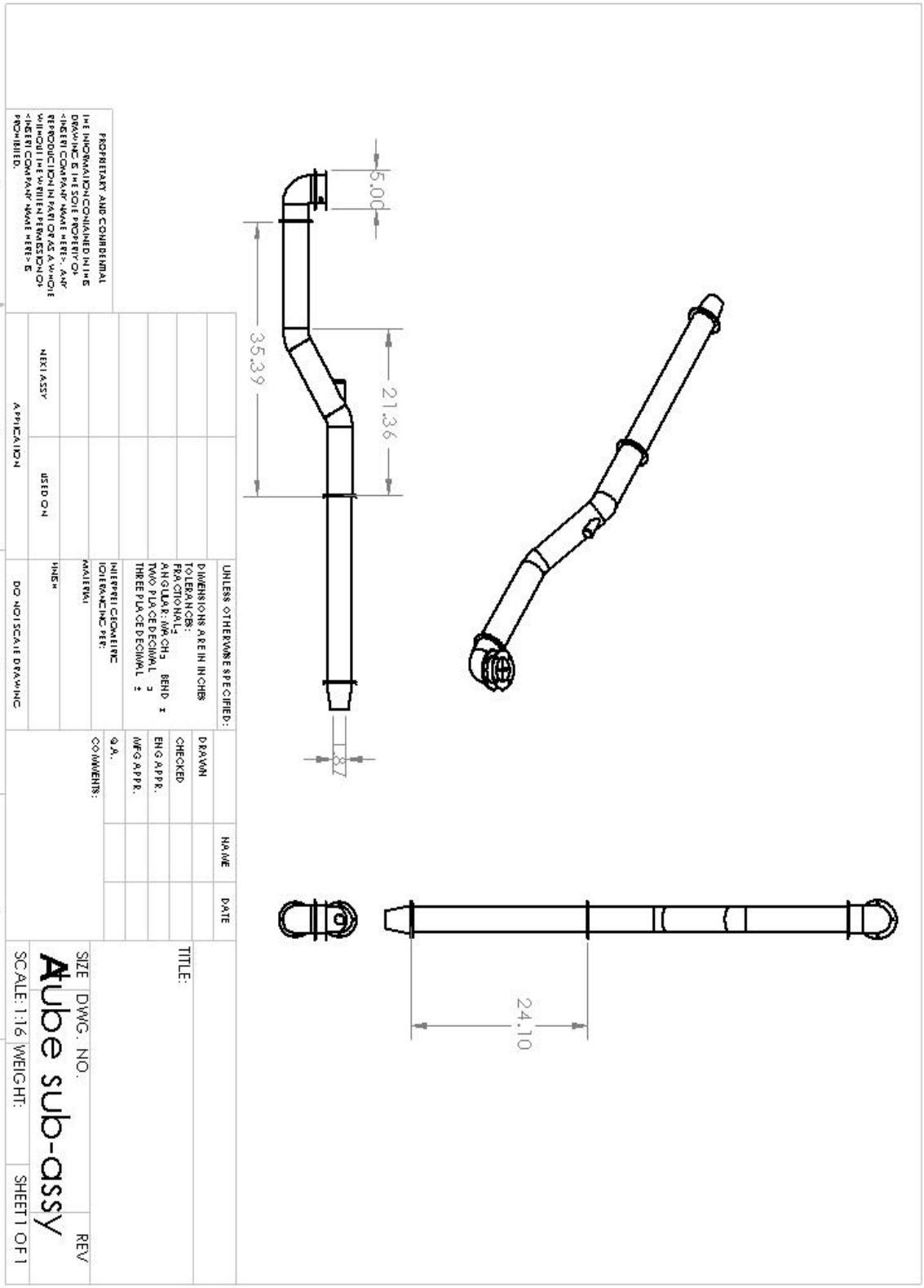

Figure 32. Schematic (Single Tube)

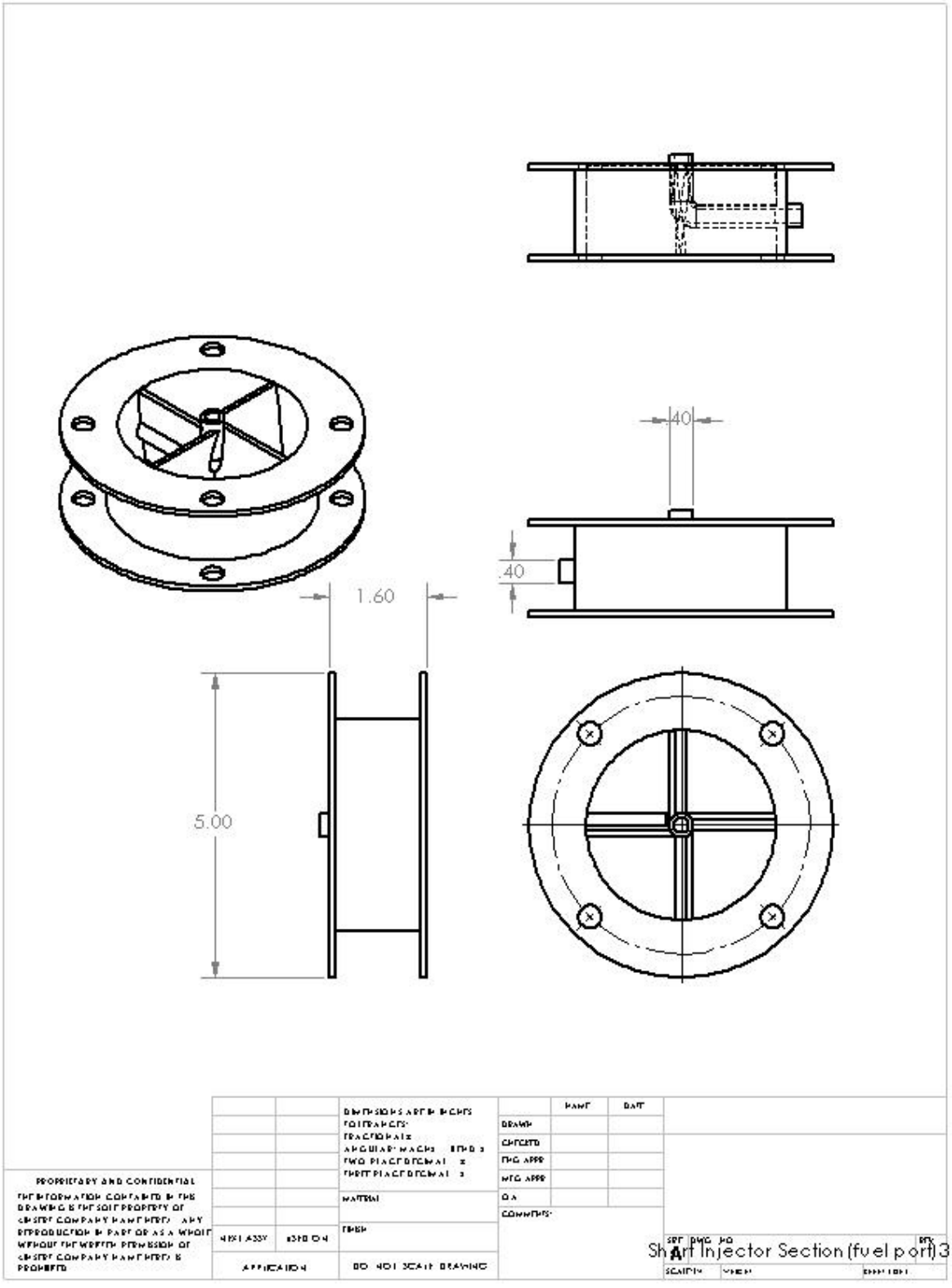

Figure 33. Schematic (Injector Section)

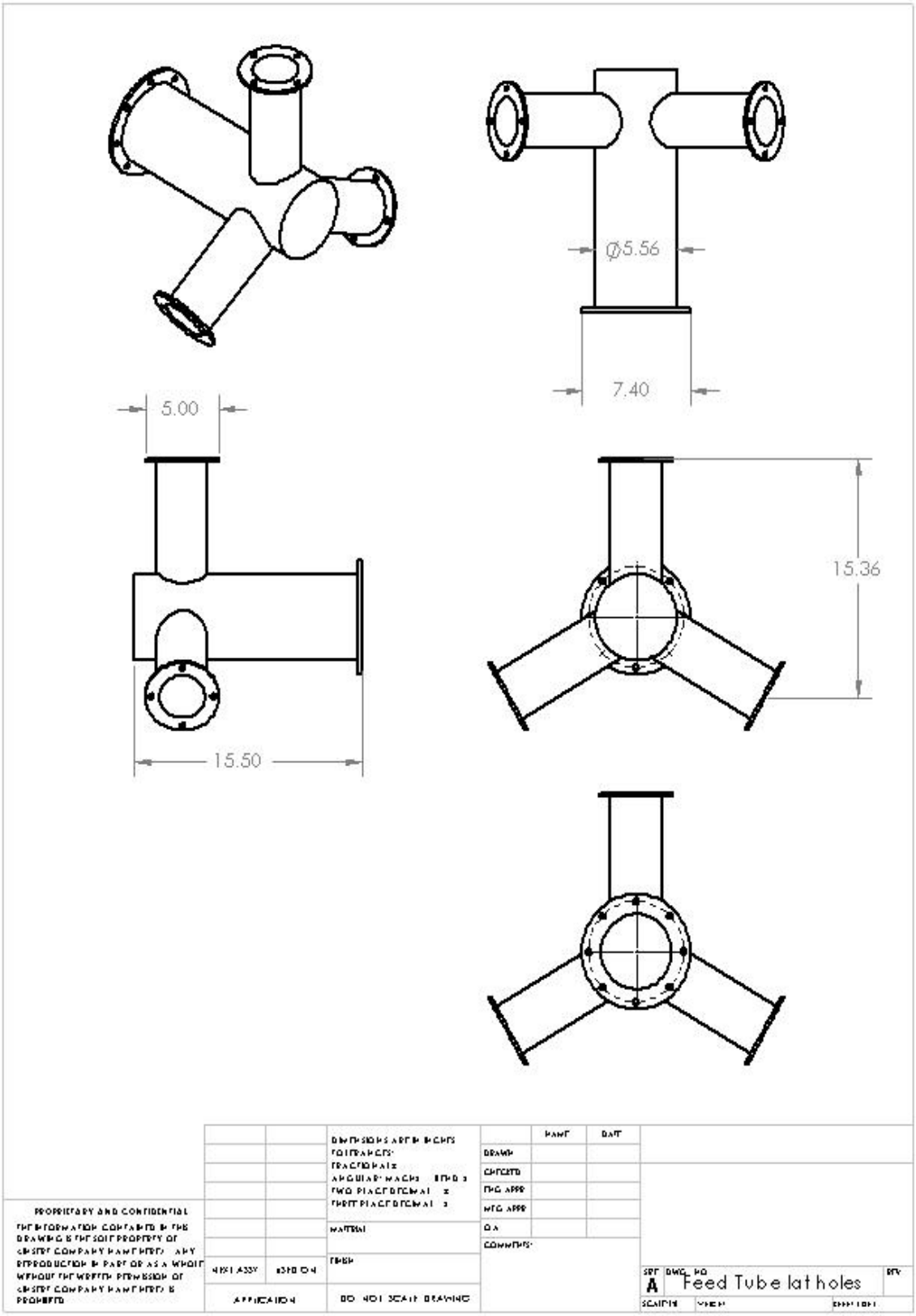

Figure 34. Schematic (Inlet Duct)

INITIAL DISTRIBUTION LIST

1. Defense Technical Information Center
   Ft. Belvoir, VA

2. Dudley Knox Library
   Naval Postgraduate School
   Monterey, CA

3. Prof. J. Sinibaldi
   Naval Postgraduate School
   Monterey, CA

4. Prof. C. Brophy
   Naval Postgraduate School
   Monterey, CA

5. LCDR B. Zittere
   Naval Postgraduate School
   Monterey, CA